2nd 9/29

NUREG - 0147
UCLA ENG - 76115

LMFBR FUEL ANALYSIS
TASK B: POST-ACCIDENT HEAT REMOVAL

FINAL REPORT
July 1, 1975 - September 30, 1976

University of California, Los Angeles
for
U. S. Nuclear Regulatory Commission

Available from
National Technical Information Service
Springfield, Virginia 22161
Price: Printed Copy $5.00 ; Microfiche $3.00

LMFBR FUEL ANALYSIS
TASK B: POST-ACCIDENT HEAT REMOVAL

FINAL REPORT
July 1, 1975 - September 30, 1976

J. Castle
I. Catton
C. Somerton
R. Wu

Manuscript Completed: November 1976
Date Published: January 1977

University of California
Los Angeles, California 90024

Prepared for the U. S. Nuclear Regulatory Commission
Under Contract No. AT(49 - 24) - 0159

TASK B
ABSTRACT

The subject of this report deals with the behavior of molten core debris following a hypothetical core disruptive accident in the proposed Clinch River Breeder Reactor Plant. Heat dissipating characteristics of an ex-vessel sacrificial bed have been analyzed. A novel form of heat transfer, analagous to film boiling, has been proposed to describe heat transfer from a heat generating pool to surrounding steel walls. Bounding type heat transfer calculations are also made to quantify such hypothetical accident characteristics as debris bed remelting, debris bed dryout in sodium and failure of the reactor cavity steel liner. Several documents that have been submitted to the NRC for its review of the CRBRP are discussed with attention being drawn to heat transfer related issues.

TABLE OF CONTENTS

LIST OF FIGURES

LIST OF TABLES

NOMENCLATURE

Br Brinkman Number

C Heat capacity

$\mathcal{D}$ Species diffusivity

d Mean particle diameter

g Acceleration due to gravity

H Molten pool depth

h Heat transfer coefficient

h_{fg} Latent heat of vaporization

h_{sq} Latent heat of fusion

h_t Debris bed transition height

k Permeability, thermal conductivity

k_a Intersticial fluid thermal conductivity

k_e Composite thermal conductivity

k_g Gas thermal conductivity

k_s Solid matrix conductivity

L Thickness

l Flow path length

Nu Nusselt Number

P Pressure

Pr Prandtl Number

p porosity

Q Heat flux

Q_v Volumetric heat generation rate

Ra Rayleigh Number

Re External Rayleigh Number

Ri	Internal Rayleigh Number
r	Radius
Sc	Schmidt Number
T	Temperature
t	Time
u	Velocity
$\bar{v}$	Mean gas velocity
x	Displacement
α	Thermal diffusivity
β	Coefficient of thermal expansion
ΔP	Pressure differential
ΔT	Temperature differential
δ	Film thickness
ϵ	Particle bed porosity
λ	Wavelength
μ	Viscosity
ρ	Density
σ	Surface tension
ν	Kinematic viscosity
$\dot{\phi}$	Steel melting rate

1. INTRODUCTION

The Division of Project Management within the Nuclear Regulatory Commission (NRC) has funded UCLA to provide assistance to the NRC staff. The specific purpose has been to facilitate the review of material submitted by the Project Management Corporation and ERDA in support of the license application for the proposed Clinch River Breeder Reactor Plant. Several general subject areas are being considered at UCLA. This annual report is concerned with Task B, Post Accident Heat Removal. The various tasks (A,B and C) all fall under the title LMFBR Fuel Analysis. The reporting period covers the time span July 1975 through September 1976. Dr. Ivan Catton is Principal Investigator for Task B. He has been assisted by research engineer Jim Castle and students Craig Somerton and Bob Wu. The work summarized in this report is a continuation of earlier contract agreements between UCLA and the NRC.

The consequences of a hypothetical core disruptive accident in a breeder reactor plant set the limits to this contract study. Emphasis has been placed on the heat and mass transfer problems that must be considered to fully understand the multiple consequences following a severe accident such as a core melt. This is a developing area of understanding and requires the best efforts of many organizations to answer a host of safety related questions. Uncertainties exist because of the high temperature, exotic materials present, and the complex nature of the physical processes. The work that is reported under Task B is analytical in nature. Reference is made in several isolated instances to UCLA generated findings. These findings are the result of test programs which the NRC's Division of Reactor Safety Research has funded at UCLA.

Coordination of the ocntract study has been with Mr. Andrew Marchese at the Nuclear Regulatory Commission (Division of Project Management). He has been provided with monthly progress letters as well as quarterly reports.

Mr. Marchese has been responsible for keeping UCLA aware of the Commission's most urgent requirements. He has also assisted in arranging information exchanges with other NRC consultants who are assisting NRC in post accident heat removal evaluations.

Four sub-tasks have been identified by the NRC within the study area of post-accident heat removal. Each of these is addressed in turn within the report. A capsule summary of each is included here.

TASK B-I: Molten Pool Propagation in a Sacrificial Layer

A bed of sacrificial material located below the reactor vessel is one means of contending with hot core debris which has melted through the vessel. Confidence cannot be placed in it as a core retention safety feature until the debris propagation in it has been understood. Section 2.0 describes several relevant topics.

TASK B-II: Heat Transfer from a Boiling Pool

A new approach has been taken by UCLA to predict the heat transfer from a boiling pool to an underlying steel support structure. This mode of energy extraction is important in establishing the extent of boiling and, thereby, the extent of fuel dispersal. Section 3.0 contains details of the new heat transfer model.

TASK B-V: PAHR Document Review

The Clinch River license applicant has submitted a large amount of safety related material to the NRC. UCLA has assisted in reviewing the portions concerned with post-accident heat removal. Specific comments pertinent to several documents, including the PSAR, are discussed in Section 5.0.

TASK B-VI: Scoping Analysis on PAHR

Bounding type calculations have been made to conservatively predict the limits of certain accident processes. The calculations are based on simple

models intended to envelop the complex nature of controlling processes. Section 4.0 illustrates the efforts carried out in this sub-task.

In addition to these four sub-tasks UCLA has worked with the Aerospace Corporation on its Technical Assistance Program. The NRC has gone to Aerospace in order to take advantage of its high temperature materials expertise. The test work is intended to clarify the nature of high temperature interactions between molten core debris, sacrificial material, and concrete. UCLA assists in providing a thermo-hydraulic input and experimental scaling. Section 6.0 is appropriate to this effort.

2.0 MOLTEN POOL GROWTH IN A SACRIFICIAL BED

The function of a sacrificial bed in the reactor cavity of a LMFBR is to provide a large capability for absorbing decay heat from hot core debris which has penetrated the reactor and guard vessels. Decay heat is to be dissipated in raising the temperature of the bed and melting a portion of the bed material. An active or passive cooling system may be present to accommodate energy reaching the side and bottom boundaries of the bed. A sufficiently large portion of the decay energy is to be taken up by the bed and cooling system so that sodium which is released also into the reactor cavity does not boil. The combination of bed material, bed size and cooling system should be such that the structural characteristics of the cavity are not degraded to a point that permits uncontrolled releases of radioactive material.

A shallow depression is customarily provided in the top surface of the sacrificial bed. The core debris is intended to drop into this depression in a predictable geometry so that recriticality can be avoided. Poison materials may be present to assist in preventing criticality. This portion of the bed must be capable of withstanding the thermal shock which accompanies the deposition of thousands of pounds of molten core debris. The molten core material creates a pool which grows outward and downward into the bed. The molten bed material should readily dissolve in the pool and dilute the hot core material.

No operating experience is available for any sacrificial bed on a large scale. Application to a proposed LMFBR is dependent on analytical predictions and scaling from small scale tests. Deficiencies which limit the accuracy of these predictions involve the paucity of high temperature properties, uncertainty in the flow pattern and resultant heat transfer at the pool boundaries, and the rate of bed material solubility.

The sacrificial bed concept has been proposed as part of the Parallel Design in the Clinch River Plant (Ref. 1, Appendix F, Amendments 5-17). An MgO refractory brick is suggested to be used in a bed 40 feet in diameter and 12 feet thick. The MgO is expected to be quite miscible in molten fuel and is approximately 40% as dense as the fuel. The license applicant has made calculations to show the extent of the expected pool growth in the MgO bed if a core disruptive accident caused the core material to melt downward and out of the reactor vessel.

The sections which follow describe efforts at UCLA to understand several aspects of sacrificial bed behavior. Independent approaches have been taken as well as a review of previously developed techniques. No overall treatment has been formulated, however, which would allow full confidence to be placed in the bed's ability to accommodate large quantities of core debris.

2.1 Sacrificial Bed Model Development

A model to describe the transfer of molten bed material to the adjacent self-heated fuel pool is currently under development at UCLA. Several objectives provide motivation for this effort. The analysis may clarify the interdependence of both heat transfer and mass transfer at the boundary. It is expected that the fashion in which fresh melt material disolves in the existing pool will have a decided impact on the distribution of the heat flux along the pool boundaries. Secondly, the equations should isolate the important groupings of physical parameters which establish the overall characteristics. These parameters will be useful in laboratory simulation tests which may be of benefit because of the difficulty in solving the general set of equations. Simulation tests have been discussed by several authors and a variety of means have been used to create a quasi-self-heated pool. Guidelines are needed in these tests to pick simulant materials having not only the proper density ratio but also an appropriate relationship between viscosity and thermal conductivity for instance. Help in choosing materials with the proper diffusion coefficient is also needed. The several paragraphs to follow will discuss the formulation of the model analysis.

A small piece has been cut from the molten pool boundary in the sacrificial bed. Figure 1 indicates how this piece is broken apart to form three contiguous layers. In the L1 layer the mass and species equations are

$$\frac{\partial \rho}{\partial t} + \frac{\partial (\rho u)}{\partial x} = 0 \qquad 2.1\text{-}1$$

$$\frac{\partial \rho_1}{\partial t} = - \frac{\partial (\rho_1 u)}{\partial x} + \frac{\partial}{\partial x}\left(\mathcal{D}_{12} \frac{\partial \rho_1}{\partial x} \right) \qquad 2.1\text{-}2$$

with D_m being the diffusivity of bed material in the fuel pool. If the materials are assumed to be incompressible the energy and momentum equations become:

$$\rho c \frac{\partial T}{\partial t} + \rho c u \frac{\partial T}{\partial x} = \frac{\partial}{\partial x}\left(k \frac{\partial T}{\partial x}\right) + \frac{4}{3}\mu \left(\frac{\partial u}{\partial x}\right)^2 + Q_v \qquad 2.1\text{-}3$$

$$\rho \frac{\partial u}{\partial t} + \rho u \frac{\partial u}{\partial x} = -\frac{\partial P}{\partial x} + \frac{4}{3}\mu \frac{\partial^2 u}{\partial x^2} + \rho g \qquad 2.1\text{-}4$$

u is the velocity in the x direction. The following dimensionless terms are used to scale the above equations.

$$t^* = t\nu_0/L^2 \qquad 2.1\text{-}5$$
$$x^* = x/L$$
$$u^* = uL/\nu_0$$
$$P^* = g_0 P L^2/\rho_0 \nu_0^2$$
$$\rho^* = \rho/\rho_c$$
$$\mu^* = \mu/\rho_0 \mu_c$$
$$T^* = T - T_s/T_f - T_s$$
$$k^* = k/k_c$$
$$D^* = D/D_0$$

The dimensionless form of the four equations of interest becomes:

Mass:

$$\frac{\partial \rho^*}{\partial t^*} + \frac{\partial (\rho^* u^*)}{\partial x^*} = 0 \qquad 2.1\text{-}6$$

Species: 2.1-7

$$\rho^* \frac{\partial m_1}{\partial t^*} = -\rho^* u^* \frac{\partial m_1}{\partial x^*} + \frac{1}{Sc} \frac{\partial}{\partial x^*}\left(\rho^* \mathcal{D}^* \frac{\partial m_1}{\partial x^*}\right)$$

Energy: 2.1-8

$$Pr\left(\frac{\partial T^*}{\partial t^*} + u^* \frac{\partial T^*}{\partial x^*}\right) = \frac{\partial}{\partial x^*}\left(k^* \frac{\partial T^*}{\partial x^*}\right) - \frac{4}{3} Br^* \left(\frac{\partial u^*}{\partial x^*}\right)^2 + \frac{Ra^*}{Ra}$$

Momentum:

$$\rho^* Pr \frac{\partial u^*}{\partial t^*} + \rho^* Pr u^* \frac{\partial u^*}{\partial x^*} = -\frac{Pr}{g_0} \frac{\partial P^*}{\partial x^*}$$

$$+ \frac{4}{3} Pr \frac{\partial}{\partial x^*}\left(\mu^* \frac{\partial u^*}{\partial x^*}\right) + Re^* Pr - Ra T^* \qquad 2.1\text{-}9$$

The dimensionless groups which appear in these equations are described here:

Schmidt No. $Sc = \nu_0 / D_0$

Prandtl No. $Pr = \rho_0 c_0 \nu_0 / k_0$

Modified Brinkman No. $Br^* = \mu_0 \nu_0^2 / L^2 k_0 (T_s - T_1)$

Internal Rayleigh No. $Ra^* = \beta g Q_v L^5 / \nu_0 \alpha_0 k_0$

External Rayleigh No. $Ra = \beta g L^3 (T_1 - T_s) / \alpha_0 \nu_0$

Modified Reynolds No. $Re^* = L^3 g / \nu_0^2$

A similar treatment applies to the L2 layer with the omission of the species equation.

The development of this model analysis is an on-going effort at UCLA. Suitable boundary conditions are being formulated and the magnitude of the six dimensionless groups are being bracketed. It is not anticipated that a general solution will be found but the relative importance of specific parameters such as the diffusivity are to be established.

2.2 Sacrificial Bed Thermal Conductivity

The specific purpose of a sacrificial bed is to absorb the fission decay energy of the core debris in the sensible and latent heat of the bed itself. This serves to reduce the net heat flux at the boundaries of the reactor cavity. Candidate sacrificial bed materials for possible inclusion in the Clinch River LMFBR are characterized by a large combination of the two heats; typically of the order 150,000 to 450,000 Btu/ft^3 of bed material. A portion of the energy leaving the molten pool in the sacrificial bed is conducted through the bed, to be disposed of by the External Cooling System (ECS) or the structural concrete heat sink. Some of the refractory materials chosen as candidates for sacrificial bed construction are porous, having a porosity of 15-25%. These pores permit the intrusion of sodium (liquid and vapor) which, because of its high thermal conductivity relative to the refractory, can significantly enhance the amount of conduction through the bed. Sodium is readily available from the large quantity which would drain from the reactor vessel in those situations wherein the sacrificial bed is required to be of service. Therefore, in order to accurately evaluate the load on the ECS and/or building parts and to quantify the bed temperature with time, it is necessary to account for sodium induced shifts in the thermal conductivity and capacity of the bed material itself.

Several investigators have studied the thermal conductivity behavior of saturated porous media. Russell (Ref. 2) proposes an empirical relationship which can be used to judge the impact of sodium in the sacrificial bed pores.

$$k_e = k_s \left(\frac{p^{2/3} + k_s/k_a (1 - p^{2/3})}{p^{2/3} - p + k_s/k_a (1 - p^{2/3} + p)} \right) \qquad 2.2\text{-}1$$

where

k_e = composite thermal conductivity

k_s = conductivity of the solid matrix material

k_a = conductivity of the interstitial fluid

p = porosity

As an example of the effect of sodium, consider the case of MgO where

k_s = 4.1 Btu/hr-ft-°F

p = .17

If liquid sodium at 1000°F is present then

k_a = 38 Btu/hr-ft-°F

The combined thermal conductivity is calculated to be 6.8 Btu/hr-ft-°F; an increase of 66% over the MgO alone. To be more complete, a range in refractory temperature should be considered since the bed temperature could vary from 300 to 4500°F. The application of the Russell approach results in the conductivity behavior shown in Figure 2. The basic MgO conductivity is taken from Reference 3 where it is made available as a function of temperature.

Figure 2 indicates a wide variation in conductivity with temperature. This information should be incorporated into any analysis which attempts to quantify the thermal load on the ECS or cavity concrete as well as establishing pool growth characteristics.

2.3 Sodium Penetration of the Sacrificial Bed

In the previous section, it was pointed out that the presence of sodium in pores of the sacrificial bed material could significantly increase the bed thermal conductivity. It is of interest then to estimate the rate at which liquid sodium can penetrate the bed itself. The depth of the MgO bed proposed in the Parallel Design for the Clinch River LMFBR is approximately 12 feet with a diameter of about 40 ft. Up to 1.2×10^6 pounds of sodium may be

released onto the bed in the bottom of the reactor cavity if the lower heads of the reactor and guard vessels are penetrated by core debris. This quantity of sodium is based on the assumption the liquid syphons from other parts of the primary heat transfer loop in addition to that contained in the reactor vessel itself. The depth of the sodium pool filling the reactor cavity would be 20 - 25 feet. Hydrostatic forces would act to cause this liquid to displace the nitrogen gas (GN_2) which fills the bed pores prior to the accident occurrence.

As a first step in the penetration analysis, it will be assumed that the nitrogen gas is not displaced from the bed pores, but only compressed. This step is taken because sodium surface tension forces would be present to resist the free exiting of the gas out the top of the bed. The magnitude of these forces is dependent upon the pore size in bed material and the extent to which sodium wets the material - factors which are uncertain at this time. Therefore, the nitrogen gas will be compressed and driven into those pores nearest the hot core debris. At 200°F and one atmosphere pressure the GN_2 density is 0.06 LB/FT^3 while at 24 psia and the same temperature the density increases to 0.10 LB/FT^3. 24 psia is the pressure which the full head of sodium would establish at the bottom of the reactor cavity. Any increase in pressure above the pool would add to this pressure. It is seen then that sodium, by compressing the GN_2, can enter about one-half the pores immediately following the sodium deluge even with no GN_2 removal from the bed. Later, as the average GN_2 temperature begins to rise, the liquid sodium might be pushed out of the bed or the GN_2 itself may be released if surface tension forces are overcome.

A manufacturer of MgO firebrick (Harbison-Walker of Pittsburg, Pa.; product name: Harklase) has provided an estimate of the material permeability based on ASTM 6577-68. Their value of 0.18 in^2/sec. psia is based on room temperature tests with air. If a correction is made for temperature (to 200°F)

and kinematic viscosity (air to liquid sodium) the permeability predicted for sodium at 200°F is 4.4 in^2/sec-psia (Ref. 4). The time required to flow 10 feet into the MgO under a driving head of 20 feet of sodium is given by

$$t = \frac{p\ell^2}{kP} = 80 \text{ sec} \qquad 2.3\text{-}1$$

where

p = brick porosity (.17)

k = brick permeability (4.4 in^2/sec)

P = driving pressure (7 psid)

ℓ = flow path length (120 in)

This quick calculation indicates that liquid sodium can very rapidly flow into the porous bed material. A more complete understanding of this process requires an understanding of the means through which GN_2 can escape from the bed, thereby permitting greater sodium intrusion.

The GN_2 escape will probably be fairly rapid. To confirm this assumption, a stability problem of the Rayleigh-Taylor type in a porous media must be solved to establish whether displacement will occur and if it will, some simple experiments must be conducted to establish the rate of penetration. The experiments can be conducted using simulants as the most important parameters are viscosity, surface tension and contact angle.

2.4 GROWS Code Implementation and Analysis

The safety analysis described in the Clinch River PSAR makes use of the computer program GROWS. This code was developed at Argonne National Laboratory specifically for predicting molten pool growth in a sacrificial bed (Ref. 5). At the request of the NRC, UCLA has acquired a copy of this code.

Minor adjustments rendered GROWS compatible with UCLA computing equipment. The logic of the code has been reviewed and test cases, appropriate to the Parallel Design for the CRBRP, have been run.

GROWS begins its analysis by assuming the molten core debris (fuel only) forms a cylindrical pool of a specified depth (subcritical) in the top of the sacrificial bed. The cylindrical, flat-bottomed geometry is maintained throughout the calculation. (Small scale experiments have not shown such an idealized geometry, Ref. 6, but this assumption is a natural first step.) The program computes a mean pool temperature at any time such that the total heat flux at the top, bottom and sidewall of the cylindrical pool matches the rate of decay heating in the pool. In each successive small increment of time the sidewall and bottom heat fluxes are consumed in raising the temperature of a certain amount of bed material to its melting point (or lowest eutectic point with UO_2) and then melting the same amount of material. The melt is assumed to mix instantaneously with the molten pool and the pool properties (viscosity, thermal conductivity, heat capacity, etc.) are adjusted accordingly. The decay power level is that shown in Figure F6.4-7 of the PSAR. The heat transfer correlations used at the three faces of the cylindrical pool are tabulated in Table I. No account is made of radiative heat transfer. Notice that the same driving ΔT is used at all three faces even though boundary conditions at the top of the pool would differ markedly from those suitable at the bottom and sidewall. Molten pool growth continues until the volumetric heat generation rate within the pool (always well mixed) drops below a specified value at which time freezing commences and the analysis stops. The criteria used to fix this minimum volumetric heat generation rate is not understood and Reference 5 includes no description of it. Consequently, GROWS is most helpful in estimating rates of pool growth and relative heat

transfer rates rather than estimating maximum pool size. No allowance is made for thermal conduction ahead of the melt front.

Table II summarizes the result of five cases analyzed by GROWS at UCLA. In each case the bed material is MgO and the core debris material was varied while the starting time (10^3 seconds after accident initiation) was held constant. An earlier starting time (500 sec) in Case 4 caused no change in penetration or freezing time but did exhibit a higher pool temperature. Reducing the area initially covered by the debris in Case 5 caused the pool to boil and the calculation process terminated. Tables III and IV are the computer output for Case 2. Figure 3 displays portions of the output of Case 2 as a function of time.

The first four cases outlined in Table II indicate the majority of the decay energy (75-80%) moves out the top of the molten pool. Furthermore, sideward pool growth continues until the bed boundary is reached in Cases 1, 2 and 4. Typically, pool freezing occurs when the ΔT driving the heat transfer process has been reduced to 2-3°C.

The pool growth calculations displayed in the Clinch River PSAR are not solely the output of the GROWS code. GROWS was used in a parametric fashion to estimate the range in downward and sideward heat fluxes (as a fraction of the total decay power). This was accomplished (see Ref. 7) by incorporating a variety of heat transfer correlations in place of those used in the standard version of the code (i.e. those of Table I). The substituted correlations were intended to account for convection caused by the addition of low density melt material from the bed. It was found that as much as 70% of the decay power could be transferred to the bed. Furthermore, the split in energy transferred to the bed into the downward and sidewall directions was observed.

GROWS was then put back on the shelf and the finite-element conduction code AYER (Ref. 8) was brought out. The 70% figure and the ratio of downward to sideward heat fluxes were inputs to the AYER code. The physical properties as computed by AYER were adjusted to allow for a latent heat of fusion when melting occurred. The code went on to compute pool growth profiles (no longer restricted to right cylindrical geometry) and sacrificial bed isotherms. Conduction ahead of the melt-front and at the bed boundaries was calculated.

Efforts are currently underway at UCLA to secure the AYER code. The author of the code has indicated that it will also be necessary to acquire the special subroutines that must be written by each user. These would be unique to the sacrificial bed application and are necessary if a thorough review of the analysis is to be completed.

Table I.

Heat Transfer Expressions Used in the GROWS Computer Code

I. Upward Heat Transfer - Volumetrically Heated Pool

$$Q_u = h_u \Delta T \qquad h_u = \frac{k}{L} Nu_u \qquad Nu_u = 0.267\ R_i^{.25}$$

II. Downward Heat Transfer - Pure Conduction

$$Q_d = h_d \Delta T \qquad h_d = \frac{k}{L} Nu_d \qquad Nu_d = \sqrt{2}\left(\frac{R_i}{R_e}\right)^{1/2}$$

III. Sideward Heat Transfer - Laminar flow over a Vertical Flat Plate

$$Q_r = h_r \Delta T \qquad h_r = \frac{k}{L} Nu_r \qquad Nu_r = 0.67733 \left(\frac{Pr}{.952+Pr}\right)^{.25} R_i^{.25} f(\phi)$$

$$\text{with } f(\phi) = 3.88/(3.88 + 13.91\phi + 46.5\ \phi^2)$$

$$R_i = \frac{\beta g Q_r L^5}{\alpha \nu k} \qquad R_e = \frac{\beta g L^3 \Delta T}{\alpha \nu} \qquad \phi = \left(\frac{R_i^2}{R_e^3 Pr}\right)^{1/2} \qquad Pr = \nu/\alpha$$

TABLE II
MOLTEN POOL GROWTH IN A SACRIFICIAL BED

OUTPUT OF STANDARD ANL 'GROWS'CODE

MATERIAL MgO
BED DIAMETER 1189 cm(39')
INITIAL POOL DIA 488 cm (16')

CASE	NOMINAL OPERATING POWER	INITIAL POOL VOLUME	STARTING TIME	MAXIMUM POOL ΔT	FINAL POOL DIAMETER	FINAL POOL DEPTH	POOL FREEZING TIME	NET HEAT FLUX DISTRIBUTION		
								UP	DOWN	RADIAL
	(MW)	(CC)	(SEC)	(°C)	(cm)	(cm)	(SEC)		(%)	
1	975	2.28×10^6	1000	300	1189*	163	22×10^6	77	9	13
2	841	1.71	1000	263	1189*	145	14	77	10	13
3	561	1.14	1000	190	1056	97	5.3	78	11	11
4	975	2.28	500	330	1189*	168	22	77	9	13
5†	975	2.28	1000	BOILING POOL						

* MOLTEN POOL GROWS TO THE SIDE OF THE SACRIFICIAL BED

† INITIAL POOL DIAMETER SET AT 345 cm. THIS RESULTS IN AN INITIAL POOL AREA 1/2 THE SIZE OF THE OTHER CASES.

CASE 2 75% OF CORE FUEL DEBRIS

INITIAL CONDITIONS

NOMINAL POWER	8.410E 02 MWT
POOL DEPTH	9.100E 00 CM
POOL VOLUME	1.[illegible]E 06 CC
STARTING TIME	1.000E 03 SEC
SACRIFICIAL BED	
MATERIAL	ESIA
LIMITING DIAMETER	1.180E 03 CM
LIMITING DEPTH	3.050E 02 CM
BULK DENSITY	3.500E 00 G/CC
HEAT OF FUSION	1.270E 03 CAL/G

TIME	H	D	DT	QD	QH	QU	Q	SORUP	VOL
1010.	9.1670E 00	4.8803E 02	2.6344E 02	2.9412E 00	1.4295E 01	2.4153E 01	3.0641E 00	6.3916E-03	1.7148E 06
2000.	9.8140E 00	4.9373E 02	1.9469E 02	2.5235E 00	1.1717E 01	1.9416E 01	2.3319E 00	5.9857E-01	1.8789E 06
3000.	1.0407E 01	4.9864E 02	1.6254E 02	2.3261E 00	1.0318E 01	1.6944E 01	1.9354E 00	1.1436E 00	2.0324E 06
4000.	1.0958E 01	5.0304E 02	1.4277E 02	2.1696E 00	9.3385E 00	1.5259E 01	1.6655E 00	1.6485E 00	2.1779E 06
5000.	1.1475E 01	5.0706E 02	1.2929E 02	2.0420E 00	8.6082E 00	1.4027E 01	1.4489E 00	2.1217E 00	2.3171E 06
6000.	1.1963E 01	5.1078E 02	1.1937E 02	1.9367E 00	8.0335E 00	1.3074E 01	1.3181E 00	2.5588E 00	2.4515E 06
7000.	1.2426E 01	5.1426E 02	1.1033E 02	1.8343E 00	7.4918E 00	1.2324E 01	1.1981E 00	2.9925E 00	2.5810E 06
8000.	1.2866E 01	5.1751E 02	1.0323E 02	1.7467E 00	7.0452E 00	1.1700E 01	1.0999E 00	3.3950E 00	2.7063E 06
9000.	1.3286E 01	5.2056E 02	9.7478E 01	1.6704E 00	6.6685E 00	1.1168E 01	1.0178E 00	3.7720E 00	2.8272E 06
10000.	1.3689E 01	5.2345E 02	9.2700E 01	1.6032E 00	6.3449E 00	1.0707E 01	9.4803E-01	4.1470E 00	2.9463E 06
20000.	1.7072E 01	5.4736E 02	6.8660E 01	1.2011E 00	4.5575E 00	8.0857E 00	5.7824E-01	7.2383E 00	4.0172E 06
30000.	1.9755E 01	5.6574E 02	5.8353E 01	9.9040E-01	3.7041E 00	6.7630E 00	4.1916E-01	9.6809E 00	4.9659E 06
40000.	2.2024E 01	5.8108E 02	5.1961E 01	8.5046E-01	3.1592E 00	5.8792E 00	3.2760E-01	1.1741E 01	5.8406E 06
50000.	2.4006E 01	5.9437E 02	4.7531E 01	7.5112E-01	2.7835E 00	5.2481E 00	2.6081E-01	1.3535E 01	6.6624E 06
60000.	2.5778E 01	6.0620E 02	4.4222E 01	6.7650E-01	2.4997E 00	4.7711E 00	2.2796E-01	1.5137E 01	7.4401E 06
70000.	2.7389E 01	6.1692E 02	4.1613E 01	6.1791E-01	2.2812E 00	4.3940E 00	1.9788E-01	1.6569E 01	8.1871E 06
80000.	2.8871E 01	6.2676E 02	3.9477E 01	5.7040E-01	2.1050E 00	4.0862E 00	1.7481E-01	1.7923E 01	8.9075E 06
90000.	3.0247E 01	6.3589E 02	3.7681E 01	5.3093E-01	1.9593E 00	3.8289E 00	1.5653E-01	1.9159E 01	9.6055E 06
100000.	3.1534E 01	6.4440E 02	3.6139E 01	4.9750E-01	1.8363E 00	3.6096E 00	1.4170E-01	2.0314E 01	1.0284E 07
200000.	4.1121E 01	7.0778E 02	2.6104E 01	3.0366E-01	1.1212E 00	2.2726E 00	6.9109E-02	2.8904E 01	1.6179E 07
300000.	4.7584E 01	7.5094E 02	2.1466E 01	2.2524E-01	8.3354E-01	1.7170E 00	4.5223E-02	3.4743E 01	2.1119E 07
400000.	5.2759E 01	7.8421E 02	1.8321E 01	1.7823E-01	6.5995E-01	1.3718E 00	3.2773E-02	3.9237E 01	2.5483E 07
500000.	5.6886E 01	8.1129E 02	1.6142E 01	1.4815E-01	5.4875E-01	1.1478E 00	2.5503E-02	4.2982E 01	2.9405E 07
600000.	6.0387E 01	8.3404E 02	1.4547E 01	1.2740E-01	4.7204E-01	9.9203E-01	2.0812E-02	4.5965E 01	3.2992E 07
700000.	6.3441E 01	8.5392E 02	1.3318E 01	1.1214E-01	4.1564E-01	8.7683E-01	1.7543E-02	4.8649E 01	3.6333E 07
800000.	6.6157E 01	8.7159E 02	1.2333E 01	1.0042E-01	3.7228E-01	7.8784E-01	1.5141E-02	5.1033E 01	3.9472E 07
900000.	6.8610E 01	8.8751E 02	1.1523E 01	9.1100E-02	3.3781E-01	7.1683E-01	1.3302E-02	5.3181E 01	4.2445E 07
1000000.	7.0849E 01	9.0204E 02	1.0842E 01	8.3500E-02	3.0970E-01	6.5871E-01	1.1863E-02	5.5141E 01	4.5277E 07
2000000.	8.6790E 01	1.0055E 03	7.3304E 00	4.7833E-02	1.7787E-01	3.8394E-01	5.6902E-03	6.9079E 01	6.8919E 07
3000000.	9.7214E 01	1.0729E 03	5.8036E 00	3.4421E-02	1.2822E-01	2.7697E-01	3.7050E-03	7.8129E 01	8.7891E 07
4000000.	1.0510E 02	1.1237E 03	4.8631E 00	2.6884E-02	1.0015E-01	2.1679E-01	2.6958E-03	8.4946E 01	1.0423E 08
5000000.	1.1144E 02	1.1645E 03	4.2157E 00	2.2165E-02	8.2546E-02	1.8082E-01	2.1051E-03	9.0422E 01	1.1866E 08
6000000.	1.1666E 02	1.1989E 03	3.7985E 00	1.9204E-02	7.1521E-02	1.5714E-01	1.7528E-03	9.5030E 01	1.2953E 08
7000000.	1.2106E 02	1.1869E 03	3.5644E 00	1.7544E-02	6.5392E-02	1.4441E-01	1.5588E-03	9.9153E 01	1.3441E 08
8000000.	1.2510E 02	1.1990E 03	3.3726E 00	1.6214E-02	6.0405E-02	1.3419E-01	1.4062E-03	1.0294E 02	1.3898E 08
9000000.	1.2885E 02	1.1890E 03	3.2116E 00	1.5119E-02	5.6446E-02	1.2577E-01	1.2936E-03	1.0644E 02	1.4307E 08
10000000.	1.3236E 02	1.1890E 03	3.0738E 00	1.4199E-02	5.3048E-02	1.1867E-01	1.1826E-03	1.0976E 02	1.4695E 08
14200000.	1.4462E 02	1.1890E 03	2.5693E 00	1.1106E-02	4.1437E-02	9.3617E-02	8.5925E-04	1.2126E 02	1.6058E 08

Time = Seconds from accident initiation
H = Pool Depth (cm)
D = Pool Dia. (cm)
DT = ΔT (^{o}C)
QH,QU= Downward, Radial, Upward Heat Flux (cal/sec-cm^2)
Q = Volumetric Heating (cal/sec-cc)
Vol = Molten Pool Volume (cc)

TABLE III. GROWS CODE OUTPUT (MgO BED)

CASE 2 75% OF CORE FUEL DEBRIS

TIME	TOTAL HEAT RATE, CAL/SEC	TOTAL HEAT CUMULATIVE, CAL	UPWARD HEAT RATE, CAL/SEC	UPWARD HEAT CUMULATIVE, CAL	RADIAL HEAT RATE, CAL/SEC	RADIAL HEAT CUMULATIVE, CAL	DOWNWARD HEAT RATE, CAL/SEC	DOWNWARD HEAT CUMULATIVE, CAL
1010.	5.2489E 06	6.6488E 09	4.5180E 06	4.5180E 07	2.0074E 05	2.0074E 06	5.3132E 05	5.3132E 06
2000.	4.3777E 06	1.1348E 10	3.7172E 06	4.0666E 09	1.7822E 05	1.8765E 08	4.8302E 05	5.0432E 08
3000.	3.9307E 06	1.5480E 10	3.3090E 06	7.5539E 09	1.6811E 05	3.6022E 08	4.5417E 05	9.7187E 08
4000.	3.6250E 06	1.9249E 10	3.0327E 06	1.0716E 10	1.6163E 05	5.2486E 08	4.3112E 05	1.4141E 09
5000.	3.4017E 06	2.2755E 10	2.8324E 06	1.3642E 10	1.5727E 05	6.8413E 08	4.1244E 05	1.8354E 09
6000.	3.2295E 06	2.6067E 10	2.6799E 06	1.6394E 10	1.5415E 05	8.3974E 08	3.9680E 05	2.2398E 09
7000.	3.0907E 06	2.9223E 10	2.5598E 06	1.9010E 10	1.5034E 05	9.9187E 08	3.8095E 05	2.6283E 09
8000.	2.9754E 06	3.2254E 10	2.4610E 06	2.1519E 10	1.4731E 05	1.1406E 09	3.6736E 05	3.0022E 09
9000.	2.8772E 06	3.5173E 10	2.3771E 06	2.3935E 10	1.4485E 05	1.2866E 09	3.5551E 05	3.3635E 09
10000.	2.7921E 06	3.8011E 10	2.3045E 06	2.6275E 10	1.4279E 05	1.4304E 09	3.4502E 05	3.7136E 09
20000.	2.3171E 06	6.3188E 10	1.9026E 06	4.7006E 10	1.3351E 05	2.8016E 09	2.8242E 05	6.8075E 09
30000.	2.0777E 06	8.5046E 10	1.7000E 06	6.4922E 10	1.2986E 05	4.1164E 09	2.4841E 05	9.4482E 09
40000.	1.9106E 06	1.0494E 11	1.5591E 06	8.1173E 10	1.2686E 05	5.3994E 09	2.2542E 05	1.1812E 10
50000.	1.7884E 06	1.2339E 11	1.4562E 06	9.6216E 10	1.2451E 05	6.6555E 09	2.0832E 05	1.3976E 10
60000.	1.6943E 06	1.4078E 11	1.3770E 06	1.1036E 11	1.2262E 05	7.8925E 09	1.9510E 05	1.5930E 10
70000.	1.6187E 06	1.5732E 11	1.3134E 06	1.2379E 11	1.2101E 05	9.1082E 09	1.8404E 05	1.7788E 10
80000.	1.5559E 06	1.7318E 11	1.2607E 06	1.3665E 11	1.1959E 05	1.0311E 10	1.7503E 05	1.9587E 10
90000.	1.5025E 06	1.8846E 11	1.2159E 06	1.4902E 11	1.1832E 05	1.1500E 10	1.6956E 05	2.1408E 10
100000.	1.4563E 06	2.0324E 11	1.1772E 06	1.6098E 11	1.1717E 05	1.2677E 10	1.6221E 05	2.3061E 10
200000.	1.1144E 06	3.2889E 11	8.9414E 05	2.6225E 11	1.0225E 05	2.3548E 10	1.1930E 05	3.6766E 10
300000.	9.5296E 05	4.3142E 11	7.6046E 05	3.4427E 11	9.3609E 04	3.3307E 10	9.9657E 04	4.7608E 10
400000.	8.3381E 05	5.2046E 11	6.6261E 05	4.1517E 11	8.5673E 04	4.2262E 10	8.6026E 04	5.6851E 10
500000.	7.4885E 05	5.9931E 11	5.9321E 05	4.7773E 11	7.9976E 04	5.0502E 10	7.6521E 04	6.4946E 10
600000.	6.8590E 05	6.7088E 11	5.4198E 05	5.3435E 11	7.4630E 04	5.8196E 10	6.9567E 04	7.2229E 10
700000.	6.3683E 05	7.3699E 11	5.0216E 05	5.8645E 11	7.0690E 04	6.5453E 10	6.4197E 04	7.8900E 10
800000.	5.9717E 05	7.9850E 11	4.7006E 05	6.3499E 11	6.7399E 04	7.2350E 10	5.9821E 04	8.5092E 10
900000.	5.6424E 05	8.5650E 11	4.4346E 05	6.8061E 11	6.4589E 04	7.8941E 10	5.6339E 04	9.0893E 10
1000000.	5.3632E 05	9.1148E 11	4.2095E 05	7.2379E 11	6.2152E 04	8.5271E 10	5.3345E 04	9.6369E 10
2000000.	3.9098E 05	1.3623E 12	3.0488E 05	1.0768E 12	4.8658E 04	1.3960E 11	3.7923E 04	1.4061E 11
3000000.	3.2498E 05	1.7166E 12	2.5221E 05	1.3524E 12	4.1954E 04	1.8457E 11	3.1086E 04	1.7473E 11
4000000.	2.8056E 05	2.0179E 12	2.1698E 05	1.5858E 12	3.7117E 04	2.2397E 11	2.6640E 04	2.0344E 11
5000000.	2.4966E 05	2.2820E 12	1.9257E 05	1.7897E 12	3.3624E 04	2.5923E 11	2.3591E 04	2.2845E 11
6000000.	2.2696E 05	2.5196E 12	1.7448E 05	1.9728E 12	3.1155E 04	2.9149E 11	2.1323E 04	2.5086E 11
7000000.	2.0938E 05	2.7373E 12	1.6034E 05	2.1398E 12	2.9560E 04	3.2181E 11	1.9479E 04	2.7121E 11
8000000.	1.9526E 05	2.9392E 12	1.4900E 05	2.2941E 12	2.8255E 04	3.5069E 11	1.8003E 04	2.8991E 11
9000000.	1.8359E 05	3.1284E 12	1.3965E 05	2.4382E 12	2.7160E 04	3.7837E 11	1.6787E 04	3.0728E 11
10000000.	1.7375E 05	3.3068E 12	1.3177E 05	2.5737E 12	2.6221E 04	4.0504E 11	1.5766E 04	3.2354E 11
14200000.	1.3862E 05	3.9386E 12	1.0395E 05	3.0501E 12	2.2344E 04	5.0368E 11	1.2331E 04	3.8031E 11

ERROR END OF FILE ENCOUNTERED ON UNIT 5 (IBM CODE IIIC217)

TABLE IV. GROWS CODE OUTPUT

3.0 MOLTEN POOL HEAT TRANSFER

The energetics characterizing a core-disruptive accident in a LMFBR can be sufficient to relocate core fuel and steel. This material might be dispersed into the upper plenum or melt and stream downward into the lower plenum. It is anticipated that the material would be particulated by sodium and settle onto the horizontal surfaces available within the vessel. If these particle beds remelt due to inherent decay heating it is possible for the molten fuel to attack the supporting steel structure. It would be beneficial to know the heat transfer rate between molten fuel and solid steel under these conditions. This information could be used to predict the time required for the hot fuel to completely penetrate the steel structure. Predicting the heat removed at this boundary is also important in evaluating the portion of the decay energy which remains available to raise the fuel temperature and possibly cause boiling of the molten pool. In certain situations the occurrence of recriticality is dependent upon whether the molten fuel is in a boiling state (lower density) or merely a molten pool (higher density). The magnitude of the pool boundary heat transfer needs to be well known because of the concerns just mentioned.

A heat transfer model has been developed at UCLA to quantify the magnitude of the energy exchange between a self-heated fuel pool and a supporting steel layer (Ref. 9). The model incorporates a Taylor instability which permits the release of immiscible steel bubbles from a liquid steel film which completely separates the solid steel from the higher density molten fuel above it. The net heat transfer is governed by conduction across the film of liquid steel. Conditions within the pool are assumed to be sufficiently well stirred to permit enough energy extraction at the bottom surface of the molten fuel pool to support a continuous film. The temperature rise across the film

prevents the fuel from freezing. Experimental evidence supporting this model has been gathered by a parallel program being conducted at UCLA for the Reactor Safety Research group at NRC (Ref. 9).

3.1 Heat Transfer Model Development

The Taylor Instability concept has been applied in the past to describe many diverse physical phenomena. Our present purpose is to show how this theory can be used to construct a model describing the heat flux from a liquid pool to a melting surface underneath, when the density of the melted phase is less than the pool density and the two fluid phases are immiscible.

Taylor first discussed in 1950 (Ref. 10) the instability of the horizontal interface between two ideal incompressible fluids of infinite depth. He showed that the irregularities at the interface tended to grow when the acceleration was directed from the heavier fluid to the less dense fluid underneath. Since that time the analysis has been expanded to include the influence of surface tension, liquid viscosity, finite depth and 3-D effects. In 1959 Zuber (Ref 11) made the first attempt to apply the hydrodynamic instability concept to film boiling on a heated surface. Zuber argued that the steady release of vapor bubbles at discrete locations in film boiling was a classical example of Taylor Instability. Using the wavelength of the "fastest growing" wave at the interface of two inviscid fluids of infinite depth and assuming two bubbles were released per cycle, Zuber was able to obtain an expression for the minimum heat flux from purely hydrodynamic considerations.

Berenson (Ref. 12) made several careful observations of the minimum heat flux for several fluids on flat plates that put Zuber's classical theory on a firm footing. Berenson also obtained an expression for the film boiling heat transfer coefficient near the minimum and an expression for the minimum temperature difference between the heater and the fluid saturation temperature which sustained film boiling.

This background work was responsible for one part of the present model development. The other part came from experimental observations described in Reference 9. Visual observations made after placing a horizontal slab of dry ice beneath a pool of warm water showed the solid surface was covered by a shiny gas blanket and CO_2 bubbles left the interface in a regular fashion. During each cycle, the interface was found to grow, collapse and regrow at the same location rather than alternate between peaks and valleys as observed in film boiling on a flat plate. The combination of dry ice and water was felt to create a situation analogous to the fuel/steel combination. The solid surface evolved a low density fluid which was immiscible in the overlying, more dense fluid. Post-test examination showed the dry ice surface to be covered by isolated peaks and valleys. The peaks (locations where bubbles were released) were on the average, one Taylor wavelength apart (approximately 2.5 cm).

The model development is premised with the following assumptions:

(i) The temperature of the liquid-liquid interface is the same as that of the upper liquid.

(ii) The solid surface is at its melting point.

(iii) A negligible amount of heat is conducted into the solid.

(iv) Liquid flow in the film toward the bubble release points is laminar.

The geometry being chosen is based on the work of Berenson (Ref. 12) and is shown in Figure 4. Only one bubble is assumed to be generated per λ^2 area per cycle*. The heat transfer across the liquid film between the bubble sites can be described by the coefficient

$$h = k_g/\delta \qquad 3.1\text{-}1$$

where k_g is the film conductivity and δ is the film thickness. We also make

* Symbols are identified in the Nomenclature section.

some additional assumptions about the film flow, bubble diameter and bubble height when released.

(v) Kinetic energy of the film liquid is small compared to the enthalpy change.

(vi) Film liquid properties are evaluated at an average temperature of the interface and the solid.

(vii) Bubble spacing is unaffected by liquid flow.

(viii) Bubble diameter is 0.4 λ and the height is 0.3 λ when released (experimental observations).

(ix) Liquid flows radially into the bubble from area λ^2.

The integrated momentum equation for the film liquid flow reduces to a form which can be written as

$$(\Delta P)_{1-2} = 7.5 \int_1^2 \frac{\bar{V} \mu_g}{\delta^2} dr \qquad 3.1\text{-}2$$

where

$$\bar{V} = \frac{k_g \Delta T}{\rho_g h_{sg} \delta^2} \frac{\lambda^2 - \pi r^2}{2\pi r \delta} \qquad 3.1\text{-}3$$

$\bar{v}$ is an average velocity within the film. Since the boundary condition on the tangential velocity at the liquid/liquid interface is not well known, the constant in Equation 3.1-2 is an average of those which apply to slip and no-slip conditions. Hydrostatically, the pressure difference between points 1 and 2 can be written as

$$(\Delta P)_{1-2} = 0.3\lambda (\rho_f - \rho_g) g - \frac{2\sigma}{0.2\lambda} \qquad 3.1\text{-}4$$

Substituting Equations 3.1-4 and 3.1-3 into 3.1-2 and integrating between point 1($r=\lambda/\pi$) and 2($r=0.2\lambda$) results in

$$0.3\lambda(\rho_f-\rho_g)g-\frac{2\sigma}{0.2\lambda}=0.3\frac{1.5\mu_g k_g \Delta T}{\rho_g h_{sg} \delta^4}\frac{\lambda^2}{\pi} \qquad 3.1\text{-}5$$

The wavelength λ of the fastest growing two-dimensional Taylor wave in inviscid fluids of infinite depth is

$$\lambda = 2\pi\sqrt{3}\sqrt{\frac{\sigma}{g(\rho_f-\rho_g)}} \qquad 3.1\text{-}6$$

Equation 3.1-5 can now be solved for δ.

$$\delta = 2.44\left(\frac{\mu_g k_g \Delta T}{\rho_g h_{sg} g(\rho_f-\rho_g)}\sqrt{\frac{\sigma}{g(\rho_f-\rho_g)}}\right)^{1/4} \qquad 3.1\text{-}7$$

This δ is that which exists between the bubble sites. If instead, a δ which is uniform over the complete surface and produces the same net conductive heat transfer were computed, it would be

$$\zeta = 2.17\left(\frac{\mu_g k_g \Delta T}{\rho_g h_{sg} g(\rho_f-\rho_g)}\sqrt{\frac{\sigma}{g(\rho_f-\rho_g)}}\right)^{1/4} \qquad 3.1\text{-}8$$

An expression for the heat transfer coefficient is finally obtained by substituting this last value for δ into equation 3.1-1.

$$h = k_g/\zeta = 0.36\left(\frac{k_g^3 h_{sg} \rho_g (\rho_f-\rho_g) g}{\mu_g \Delta T \sqrt{\sigma/g(\rho_f-\rho_g)}}\right)^{1/4} \qquad 3.1\text{-}9$$

This completes the description of the heat transfer model and the expressions which are an outgrowth of it. The melting process has been analyzed as a pseudo-film boiling mechanism. The next section will describe experimental evidence which was gathered to support various aspects of the model.

3.2 Experimental Evidence in Support of Heat Transfer Model

Simple bench-top experiments have been conducted using readily available materials. The work was supported by the Reactor Safety and Research Division within the NRC (Ref. 9). Experimental measurements of the heat transfer from a pool of warm water or benzene to an underlying slab of dry ice were per-

formed in the steady state (pool temperature held nearly constant) and the quasi-static state (pool temperature varying with time.) These combinations resulted in a gas layer separating liquid and solid rather than a liquid as would be the case with the fuel and steel. However, the basic features of the model as built upon the Taylor instability are present. The density ratio of the two fluids was approximately 400 in the tests whereas 1.3 applies to fuel and steel. Laboratory work at Argonne (Ref. 13) indicated that the Taylor Instability process is present when immiscible materials having nearly the same density are used. The Argonne tests utilized glycerin as the overlying fluid and wax as the melting solid. The present test apparatus is shown in Figure 5. The apparatus included a thick horizontal sheet of styrofoam for supporting the dry ice slab. The liquid pool was held within a thin sheet metal cylinder covered on the sides with foam insulation and open on both ends. A sponge rubber sealing gasket with a loading collar was attached to the cylinder. A provision for placing a cartridge heater in the cylinder was also made so that in steady state experiments the pool temperature could be maintained constant by controlling the power to this heater. The pool temperature was measured by a copper constantan thermocouple. About two kilograms of distilled water or benzene was heated on a hot plate. The temperature and weight were noted and then the test liquid poured into the sheet metal cylinder. The depth of the liquid pool varied from 11-14 cm. Agitation caused by the rising gas bubbles kept the temperature very uniform within the pool.

In the steady state experiments the heat transfer rate from the pool was estimated and power to the cartridge heater was adjusted accordingly. The temperature of the pool was recorded as a function of time using an X-Y recorder. The power input from the heater was used to calculate the rate at which energy was lost from the pool. If the initial estimate for the power setting was slightly off the energy loss from the pool was corrected by noting the time rate of change in the pool temperature and an average pool temperature

was then used in the heat transfer calculations. If the initial estimate was off by a significant margin a new test with an adjusted power setting was made. Error analysis showed that the heat loss calculations were accurate within ±3%.

In the quasi-static tests, the heater was not used. Heat transfer calculations were made by noting the rate of change of the liquid enthalpy (based on mass, specific heat, and temperature change). The error in the quasi-static heat flux calculations was found to be less than ±2%.

Observations of the gas temperature as it left the free surface showed that the gas exited at the pool temperature. During the course of the experiments it was observed that a significant amount of heat was lost from the pool by evaporation at the pool surface and into the gas bubbles. It was very difficult to ascertain these heat losses theoretically, hence heat loss correction data were obtained by carrying out simulated experiments without the dry ice. In these experiments nitrogen gas at a known volumetric flowrate was released from a bubble manifold at the bottom of the pool. The heat loss curves at different pool temperatures and gas flow rates were obtained from the time rate of change in the pool temperature. The raw heat transfer data were then corrected for heat losses to the surroundings. The apparent uncertainty in applying this correction for evaporative cooling is approximately ±15% at the highest water temperature. Altogether, the heat loss from the pool can be isolated into several categories.

(i) Conduction into the dry ice slab.

(ii) Energy used to cause dry ice sublimation at -79°C.

(iii) Heating CO_2 gas to the pool temperature.

(iv) Energy consumed in liquid evaporation.

(v) Conduction into the apparatus.

Item (i) is assumed to be negligible while item (ii) is the ultimate quantity to be determined. Item (iii) is accurately known once the pool temperature is measured. Items (iv) and (v) are measured simultaneously in the simulated experiments just described.

The mass transfer from the dry ice surface caused the originally flat surface to become uneven with time. This in turn resulted in the exposure of more surface area to the liquid pool. For this reason the data reported are for early periods of time (less than 2-3 minutes) when the subliming surface was relatively flat.

3.3 Test Results and Discussion

The dry ice surface after exposure to warm water for a long period of time (15-25 minutes) was found to be very uneven. The peaks and valleys on the surface displayed a regular pattern and were found to be arranged in a roughly square pattern with the peaks spaced a Taylor wavelength apart. The distance between peaks was approximately 2.8 cm whereas for water at 298°K Taylor Instability theory predicts the wavelength of the "fastest growing" two-dimensional Taylor wave to be 2.85 cm. The peaks on the dry ice surface correspond to the nodes where a bubble grew and departed at regular intervals. Because of the very small heat transfer to the dry ice beneath a growing bubble the sublimation rate of the dry ice is small. This effect accumulated over a period of time gives rise to the formation of conspicuous peaks. The height difference between the peaks and valleys seemed to reach a steady state limit ($\sim\lambda/3$).

The corrected steady state and quasi-static heat flux data for water are plotted in Figure 6 as a function of the temperature difference between the water and the sublimation temperature of the dry ice. The steady state data tend to show larger scatter because of increased uncertainty associated with the heat flux calculation when the initial estimate of the heater power was

not correct. The curve faired through the data shows a knee at $\Delta T = 87°K$ (water temperature = 287°K). Visual observations showed that below this temperature a stable gas film was no longer sustained and partial, direct contact of water with the dry ice was established. The heat flux quickly drops to nearly zero after the gas film breaks down and the water reaches its freezing temperature.

The heat transfer coefficient data are plotted in Figure 7. In this figure the predictions for the laminar film heat transfer coefficient based on Berenson's formation as well as Equation 3.1-9 are also shown. In the stable film boiling, the heat transfer coefficient is weakly dependent on temperature for ΔT varying from 87 to 108°K. In this region the data are well correlated by our prediction while Berenson's prediction is about 15% higher. At temperatures higher than 108°K the heat transfer coefficient is strongly dependent on temperature. In this region the coefficient is probably increased by the turbulent nature of the film.

The quasi-static heat transfer coefficient data for benzene are plotted in Figure 8. For ΔT greater than 97°K (benzene temperature = 291°K), the coefficient depends weakly on temperature and the data are correlated by Equations 3.1-9. The stable film breaks down below $\Delta T = 97°K$ in that region where the film collapses and allows the benzene to freeze.

The non-dimensional heat transfer data for stable pseudo-film boiling are plotted in Figure 9 as a function of Reynolds number. The heat transfer coefficient is independent of the Reynolds number in the laminar region. In the turbulent range, the heat transfer coefficient varies as $Re^{1/2}$. The dimensionless heat transfer coefficient for constant Prandtl number ($Pr \sim 0.7$) can be written as

$$h\lambda/k_g = 245 \qquad Re < 40 \qquad 3.3\text{-}1$$

$$h\lambda/k_g = 37.5\ Re^{0.5} \qquad Re > 40 \qquad 3.2\text{-}2$$

The value of the transition Reynolds number in the gas films is considerably lower than in pipes. This may be due to the presence of a slip condition at the liquid-gas interface which allows for turbulence to more readily develop in the major portion of the film.

The minimum ΔT required to maintain a stable gas film in the water and benzene tests is considerably lower than that predicted by Berenson. Berenson predicts 144°K for water and 87°K was measured. 114°K was predicted for benzene and 97°K measured. Additional work must be conducted to clarify this discrepancy.

The experiments described in Reference 9 with water and benzene which have been summarized here have provided new insight into heat transfer processes which have application to the molten fuel/steel combination that develops after a core disruptive accident. The model suggests that a continuous thin film of liquid steel could separate the molten fuel and solid steel. Bubbling release of the lower density steel would result in uneven erosion of the solid surface by melting. Additional experimental work is required using materials which have properties more closely approximating those of fuel and steel. The minimum film ΔT required to maintain the process is also not clearly understood at this time. The tests do, however, indicate that the major model features, a pseudo-film boiling process, are accurate.

3.4 Model Application to LMFBR Conditions

It has been argued that the heat transfer model developed in the previous sections can be applied to situations arising out of a core disruptive accident. The conditions most likely to fit the model occur when molten fuel is supported by a horizontal steel surface. The following additional assumptions will be made.

(i) A direct contact of molten UO_2 and steel exists--no fuel crust is present.

(ii) Heat is transferred by conduction from the fuel through a molten steel layer and is utilized to melt the steel.

(iii) The agitation of the rising steel bubbles keep the molten fuel well mixed and uniform in temperature.

(iv) The melting temperature of UO_2 is lower than the boiling point of steel, but is greater than the minimum ΔT required to establish a stable steel film.

With these assumptions the average heat transfer coefficient from fuel to steel is given by Equation 3.1-9 which is rewritten here.

$$h = 0.36\left(\frac{k_g^3 h_{sg} \rho_g (\rho_f - \rho_g) g}{\mu_g \Delta T \sqrt{\sigma / g(\rho_f - \rho_g)}}\right)^{1/4}$$

For a UO_2 pool temperature of 3150°K and a steel melting temperature of 1700°K (ΔT = 1450°K), Equation 3.1-9 results in

$$h = 62 \text{ kw/m}^2\text{-K}$$

or

$$q = 90 \text{ mw/m}^2$$

This heat flux corresponds to an average steel melting rate of approximately 1.7 cm/sec. For a full-power heat generation rate of 150 w/g, Equation 3.1-9 is valid as long as the fuel pool depth meets the criteria

$$H \geq 0.06/f \quad [\text{m}] \qquad 3.4\text{-}1$$

(where f is the fraction of full power) and all the boundary heat transfer is occurring at the lower surface.

The computed melting rate of the underlying steel is very high and at least an order of magnitude higher than the most conservative estimates that have been made so far. This new development has strong implications in terms

of the downward movement of core debris and the extent to which energy will be available to cause boiling in the core region. As such, these considerations raise safety related issues and will continue to receive attention.

4.0 SCOPING ANALYSES ON PAHR IN THE CLINCH RIVER LMFBR

One of the PAHR contractual tasks called out for FY 1976 requires that scoping analyses be performed at UCLA. The objective of this task is to conservatively bound the thermal behavior of processes taking place during post accident heat removal. This information, in turn, will be used to assess the safety adequacy of the proposed PAHR design concepts for the Clinch River LMFBR Plant. Specific considerations which are not well defined and can benefit from a bounding-type calculation include the extent of in-vessel cooling capability, thermal response of the reactor cavity, the vessel penetration time and the maximum penetration of molten core debris into sacrificial material or concrete.

4.1 Reactor Cavity Linear Penetration

Many of the equipment cells in the concrete structure below the containment building in the proposed Clinch River Plant are fully lined with steel membranes ($\sim$1.0 cm thick). The liner serves several purposes. First, it more readily contains an inerting nitrogen cell atmosphere than would the porous concrete. Secondly, it facilitates clean-up operations if sodium is spilled and thirdly it isolates, and hopefully prevents, the direct contact of sodium and concrete. The interaction of concrete and sodium can be vigorous with large quantities of gases and energy being generated. Several steel liner designs have been suggested with differences being found in the separation from the concrete and the presence of several types of insulation between the liner and the concrete.

Molten fuel at high temperature ($\leq$3000°C) may be released from the reactor and guard vessels following a core disruptive accident. This material is sufficiently energetic that it can melt through the vessels and then flow out

through the failure points. The molten material would drop (2-3 m) directly onto any steel liner which was placed on top of the reinforced concrete reactor cavity floor. One of the plant designs which incorporates such a liner is described in Reference 14. Special provisions are made to accommodate the thermal expansion of the liner as it is heated by the core debris (fuel, steel and sodium).

A very large heat transfer coefficient is established at the stagnation point where the streaming fuel impinges on the steel liner. The melting rate and erosion of the steel itself would be correspondingly high when the large ΔT involved is also considered. Liner failure would permit molten fuel to flow beneath the liner and along various vent passages in that region. The accumulation of fuel beneath the liner could be enhanced if the liner warped due to thermal stresses. This entire process may take place before sodium is released through the failure in the guard vessel and subsequently quenches the fuel and steel debris that had already been deposited in the reactor cavity. Fuel in isolated regions beneath the liner would not readily particulate in which case sodium would not be as effective in removing decay heat as it is when a fully wetted debris bed is formed of fuel and steel particles in sodium.

To estimate the magnitude of the heat transfer coefficient at the stagnation point on the liner it is necessary to make several simplifying assumptions. A nominal jet diameter of 20 cm is taken and a free fall height of the stream is taken to be 2 m. The jet diameter would actually be established by the time-dependent hole size in the reactor guard vessel. Material properties for the fuel are those applicable to UO_2 near its melting point (2850°C).

$$Re = \frac{\rho V R}{\mu} = \frac{8400\ kg/m^3\ (6.3\ m/sec)\ 0.1\ m}{.005\ kg/sec\text{-}m} = 10^6$$

$$Pr = \frac{C_p \mu}{k} = \frac{500\ J/kg\text{-}°K\ (.005\ kg/sec\text{-}m)}{3\ J/m\text{-}sec\text{-}°K} = 0.8$$

4.1-1

Reference 15 is helpful in quantifying the heat transfer coefficient given the jet Reynolds and Prandtl numbers. The referenced material is based on laminar flow whereas the actual jet Reynolds number above indicates turbulent conditions will develop. Therefore, turbulent augmentation should create a larger heat transfer coefficient than computed here.

$$Nu = 0.36\ Re^{0.5}\ Pr^{0.37} \qquad 4.1\text{-}2$$

$$Nu = hR/K = 345$$

$$h = 10^4\ J/m^2\text{-}sec\text{-}°K$$

A nominal ΔT between the jet and the steel liner is taken to be 2850-1450 = 1400°C. The added assumption is made that the jet very effectively flushes away any molten steel which might otherwise serve as an intervening, insulating layer. The rate of melting attack ($\dot{\phi}$) is then given by:

$$\dot{\phi} = h\Delta T/\rho h_{sf} = \frac{10^4\ W/m^2\text{-}°K\ (2500°K)}{7500\ kg/m^3\ (270 \times 10^3\ W\text{-}sec/kg}$$

$$\dot{\phi} = 1\ cm/sec \qquad 4.1\text{-}3$$

All the heat transfer is assumed to cause steel melting. The magnitude of $\dot{\phi}$ indicates that the floor liner (3/8" steel plate) should fail in the first few seconds during which it experiences the harsh environment of the molten fuel stream. Subsequently, the insulation and/or concrete beneath will be subject to an aggressive attack.

4.2 Core Debris Bed Remelting

Following a core disruptive accident in a LMFBR the hot core debris (fuel and steel) may melt downward through the core support structure and

drop into the lower inlet plenum. It is anticipated, based on small-scale laboratory tests, that the core debris would be particulate during the rapid quenching action occurring in the sodium filled lower plenum. The laboratory tests which simulated this thermal interaction have quantified the range in particle size and porosity of the particulated debris (Ref. 16). Typically, particle sizes for UO_2 range from 100-1000 microns with a porosity of approximately 50%. The particles are assumed to be quenched to the final sodium pool temperature during this process. In the Clinch River Plant the bulk temperature of the debris and sodium is estimated to be 1075°F immediately following the quench (Ref. 1).

The decay heat output of the core debris is sufficient to remelt the debris if the net heat transfer to the sodium bath and surrounding structure is sufficiently small. It is possible to compute a minimum debris bed remelt time if all the decay energy is assumed to contribute only to heating the fuel and steel particles and drying out the bed (evaporating sodium). The energy taken up by this process serves to delay the onset of molten debris attack on the lower head of the reactor vessel.

A calculation of the debris bed remelt time has been made for the following set of conditions:

(i) The bed consists of a homogeneous mixture of UO_2 and stainless steel.

(ii) The initial temperature is 1075°F.

(iii) Bed porosity is 50%.

(iv) All the decay energy generated is consumed in sensible and latent heat of sodium, UO_2 and steel.

(v) Uniform conditions exist at any time throughout the bed. The physical properties used in the calculation are listed in Table V.

TABLE V

Debris Bed Physical Properties

	T_{melt} (C)	T_{boil} (C)	ρ_{solid}	ρ_{liq} (kg/m^3)	ρ_{vap}	C_p (kJ/kg-C)	h_{fg} (kJ/kg)
UO_2	2850	---	10000	---	---	0.45	280
S.S.	1410	---	7600	6600	---	0.75	270
Na	---	880	---	740	0.0	1.3	3880

Calculations have been made of the energy required to raise the bed to two final conditions. Figure 10 shows the energy required to reach 1410°C and remelt the stainless steel in the bed. Figure 11 is the total energy required to heat the three materials to the fuel melting point and then remelt the fuel as well. Only that amount of sodium vapor required to fill the voids in the debris bed is vaporized.

In order to relate these remelt energy requirements to an elapsed time for remelting the integrated decay power curve contained in the Clinch River PSAR is utilized (Ref. 1, Fig. F6.5-8). In the time period 10^1 to $6x10^3$ seconds following accident initiation (e.g. loss-of-flow with failure to SCRAM) the integrated power curve is approximated by the linear expression:

$$\log Q[B] = .860 \log t[sec] + 5.05 \qquad 4.2\text{-}1$$

where Q is the <u>total</u> decay heat generated as a function of time t. Figure 12 indicates the elapsed time required to generate a given amount of decay heat starting at a predetermined time. This curve can still be used even if the entire amount of core fuel is not present. One notes for example, that the time required for 1/2 the fuel debris to generate $5x10^7$ Btu is equal to the time required for the full fuel load to generate $2 x(5x10^7) = 10^8$ Btu.

Figures 10, 11, and 12 can be used in conjunction then to estimate remelt time. Once the debris quantity is known Fig. 10 or 11 details the necessary

energy input. Figure 12 then specifies the time required to accumulate this amount of energy through fission decay heating.

4.3 Shallow Debris Bed Dryout

The scenarios proposed to describe the consequences of a core disruptive accident are varied in nature. A common feature, however, is the interaction of molten fuel and/or steel with subcooled sodium leading to fragmentation into small particles. These fuel and steel particles may settle on various horizontal surfaces within the reactor vessel surrounded by a bath of sodium. If the heat generation rate in the particles is sufficiently high the bed of particles will dryout due to a deficiency in coolant supply. Subsequent remelting of the fuel particles could lead to failure of the underlying steel structure and possibly the failure of the primary containment. It is of interest then to know the extent to which particle beds can remain wetted by sodium as a function of the volumetric heat generation rate.

Several authors have described their work on debris bed dryout (see, for example Ref. 17). Both analytical and experimental programs are common. Work at UCLA was described in Reference 17 which detailed a project funded by the Nuclear Regulatory Commission. Efforts have continued at UCLA to understand the behavior of shallow debris beds. This type of bed is characterized by the formation of narrow and distinct vapor channels which penetrate the full depth of the bed. Vapor channels are present in deep beds but do not reach the bottom surface. Reference 17 contains a prediction of the dryout heat fluxes in deep beds which may form in the CRBRP. Recently, Dhir published an analysis of shallow bed features based on his work at UCLA (Ref. 18). The comments which follow in this section are intended to illustrate the application of Dhir's treatment to shallow beds in the CRBRP. The reader should

note that the term shallow does not imply that this type of bed is always less deep than a deep bed. Porosity, particle size and heat generation rate disrupt this notion.

In a shallow particle bed the solids are in a fluidized state and the coolant has easy access to all regions within the bed. A hydrostatic pressure head equal to the bed height drives vapor out along the vertical channels. If the vapor velocity exceeds a critical value, the jet in the overlying fluid will become unstable and break down, leading to choking of the exiting flow. The choking action would inhibit the supply of coolant, thereby leading to dryout. The dryout heat flux in the particles is established by conditions existing in the vapor jets above the bed. When Dhir considered this model in detail he arrived at an expression for the dryout height (h) as a function of the volumetric heat generation rate (Q_V), bed porosity (ε) and fluid properties. No dependence on particle size was found (in contrast to deep bed analysis). For the shallow bed situation:

$$\frac{Q_v h(1-\varepsilon)}{q_z} = 1.84 C_4 \left\{ 1 - C_5 \frac{h(1-\varepsilon)}{\sqrt{\sigma / g(\rho_f - \rho_g)}} \right\} \qquad 4.3\text{-}1$$

where

$$q_z = \frac{1}{24\pi} \sqrt{\rho_g}\, h_{fg} \left\{ \sigma g (\rho_f - \rho_g) \right\}^{1/4} \qquad 4.3\text{-}2$$

A test program was conducted which suggested values for the empirical constants C_4 and C_5.

$C_4 = 0.33$

$C_5 = 0.092$

The constants were selected to conservatively encompass the data scatter exhibited by the test results. This conservatism is influenced by the test experience with deep beds also.

If we make specific reference to liquid sodium at one atmosphere.

$$\frac{q_z}{\sqrt{\sigma / g(\rho_f - \rho_g)}} = \frac{34 \text{ cal/sec-cm}^2}{0.4 \text{ cm}}$$

When sodium properties were inserted into the expression for dryout in deep beds (Ref.18) the result was

$$h = \frac{0.31 \times 10^4 \bar{d}^{-2}}{P} \left(\frac{\varepsilon}{1-\varepsilon}\right)^3 \text{ [cm]} \qquad 4.3\text{-}3$$

with $\bar{d}$ = mean particle diameter in microns

P = percentage full power (full power = 150 w/gm)

The transition height (h_t) between the shallow and deep bed regimes can be found by substituting 4.3-1 into 4.3-3 and noting that Q_v in cal/sec-cc is approximately equal to 3P. If $\varepsilon = 0.5$ then

$$h_t = 8.6 - 1.9 \times 10^{-5} \bar{d}^2 \text{ [cm]} \qquad 4.3\text{-}4$$

It is now possible to compare the UCLA dryout results with those suggested in the Clinch River plant PSAR (Ref. 1). Specific reference is made to Tables F6.4-1 (Amend. 5) and F6.4-1A (Amend. 17). A comparison of the two predictions sets is readily apparent in Table VI. In each case the limitations as established by the UCLA analysis are for shallow beds. This would be true as long as the mean particle diameter is less than ~ 450μ. A larger mean would increase the stable depth. In each instance the UCLA prediction is about 1/3 of that shown in the PSAR. The very narrow band of conditions considered prevents a determination of the differences in general (i.e. at other heating rates and porosities). The lower UCLA values may be due to the conservatism in selecting empirical constants so that the test data is bracketed. The data scatter is mostly likely a reflection of the fact that a role is played by factors which are difficult to control such as size distribution, trapped gases, and particle irregularities.

In the time period 30 to 200 seconds following subcriticality the heat generation rate in the debris is 3 1/2 to 5 1/2% of full power. The stable bed

heights are fixed by the shallow bed characteristics which are independent of particle size. The UCLA analysis is not able to confirm the PSAR statement that added fines would increase the stable height (as reflected in Table F6.4-1A).

TABLE VI
Dryout Heat Flux Conditions-Stable Depths

Time from Subcriticality (sec)		Full Decay Heat: 50 % steel	70% Decay Heat: 50% steel	Full Decay Heat: 100% oxide	70% Decay Heat: 100% oxide
30	PSAR	11.2 cm	12.4	7.1	9.1
(P=5.3)	UCLA*	3.3	4.0	2.1	2.6
100	PSAR	11.9	13.2	8.6	9.9
(P=4)	UCLA*	3.9	4.7	2.5	3.2
200	PSAR	12.3	13.7	8.9	10.1
(P=3.5)	UCLA*	4.2	5.0	2.8	3.4

*$\bar{d} \leq 450\mu$

5.0 DOCUMENT REVIEW

One of the program tasks at UCLA has been a technical document review for the LMFBR Branch (NRC's Division of Project Management). The material that has been under consideration for this task during FY 1976 consists of that information submitted to the NRC as part of the Clinch River LMFBR licensing procedure. A selected portion of those reports referenced in the submitted material have also been the subject of review. The review topics encompass the heat and mass transfer considerations pertinent to the hypothetical core disruptive accident. These areas of interest fall under the general title of post-accident heat removal (PAHR). The word accident, in this case, refers to a major core disruptive event. Specific items include the extent of core dispersal, debris bed dry-out, molten fuel pool heat transfer and melting penetration of steel, concrete and sacrificial barriers.

The Preliminary Safety Analysis Report (PSAR) (Ref. 1) is the primary means by which the applicant forwards details of the proposed Clinch River Plant to the NRC. Appendix F within the PSAR contains a treatment of the plant operations during a hypothetical core disruptive accident. Careful consideration is given in the PSAR to the procedures and plant features which are intended to minimize radiation leakage to the environment. As such, the heat transfer related problem areas in the hypothetical core disruptive accident have been reviewed. Supporting documentation published by Westinghouse and Argonne laboratories was also the subject of review.

The special plant features described in Appendix F, applicable to a core-disruptive accident alone, in conjunction with the rest of the proposed plant, form the so-called Parallel Design. The base-line design in the absence of these features is the Reference Design. Amendment 18 to the PSAR (April, 1976, Ref. 19) requested that the Parallel Design be withdrawn from

consideration by the NRC staff; stating that future emphasis was to be on a single Reference Design. The applicant felt the Reference Design was a balanced approach to safety and focused on preventing the low probability initiators of severe accidents. Furthermore, the Reference Design was felt to provide the capability to mitigate the consequences of low probability severe accidents when treated on a realistic basis.

Several plant features were added in Amendment 18 to the Reference Design to provide additional safety margin in the event of a core disruptive accident. Some of these items are the reactor cavity venting system, a containment clean-up filtration system, a low-leakage containment building and a containment air purge system. A more detailed description of the amended features is available in Reference 14. This document has been reviewed for the benefit of the NRC staff.

The objectives of the review process have been multi-fold. Included are:

(i) Clarification of those aspects of the design not clearly identified in the submitted material.

(ii) Verify heat transfer related calculations. (This overlaps the work described in Section 4.0)

(iii) Identify those analyses which would be more accurately treated in a different fashion.

(iv) Identify omissions and describe why additional work is needed.

The following sections will outline the outcome of the review process when applied to Appendix F of the PSAR and the Reference Design as augmented by the third level thermal margins.

5.1 NRDC Interrogatories

The National Resources Defense Council (NRDC) et al have initiated legal action in order to raise various contentions they wish to be considered during

the safety and environmental review hearings for the CRBRP. As part of this action they have submitted interrogatories to the NRC on several occasions. The NRC has asked UCLA to assist in responding to those NRDC questions which are PAHR related. In general the subject areas are those discussed in Appendix F(Amendment 5-17) of the PSAR (Ref. 1) and are concerned with clarifying the state-of-the-art and identifying organizations knowledgeable in particular areas. UCLA has provided a specific response to the NRC in two instances (Ref. 20 and 21) during FY 1976.

5.2 Third Level Thermal Margins

The NRC considers three levels of design when evaluating the safety adequacy of a proposed nuclear power plant design. The first level entails a sound design intended to provide high reliability and to minimize the occurrence of accidents. The second level includes plant features which protect against failures or malfunctions anticipated to occur despite precautions. Additional public protection is provided by third level design features even in the event of the extremely unlikely consequences of hypothetical failures. The combination of these elements is referred to as defense-in-depth. The applicant for the Clinch River Plant license is endeavoring to provide margin against events beyond those included in the extremely unlikely category. The applicant believes the public health and safety can be protected even if the reactor primary coolant boundary is breached. The most current description of the plant features that provide third level margins is found in Reference 14. The contents of this section will pertain to the description contained in this reference report. Note that the plant features described here differ from those contained in the Appendix F material (Amendment 5-17 of the Clinch River PSAR, Ref. 1)

The design features added to the basic Reference Design to enhance the third level margin are shown in Figure 13. The added items include:

(i) A reactor cavity vent to the containment building.

(ii) Steam and CO_2 vent provisions behind the reactor cavity steel liner.

(iii) Containment building clean-up provisions (vent, purge and filtration).

(iv) Air cooling of the containment annulus.

(v) Dual control room air intakes.

(vi) Associated instrumentation and radiation monitoring systems.

Each of the listed items plays an active or passive role following the release of core debris from the reactor vessel in the event of a core disruptive accident. The term Inherent Retention is sometimes associated with this newest concept to distinguish it from the original Reference and Parallel Designs approaches.

The Inherent Retention design is specifically laid out to contain a core disruptive accident as described in this scenario:

(a) Core debris (fuel, steel, sodium) melts through the reactor and guard vessels 1000 seconds after the initiation of a core disruptive accident (e.g. loss-of-flow without SCRAM).

(b) The hot debris immediately penetrates the floor steel liner. The fuel and steel debris particulates and self-levels across the 40' diameter floor.

(c) The reactor cavity is vented into the large containment building at four hours to prevent cavity overpressurization.

(d) The containment building is vented to the atmosphere through a filtration system at six hours to prevent overpressurization and excessive hydrogen gas accumulation.

(e) Sodium begins to boil in the reactor cavity and is vented into the containment building where it reacts with air and water vapor.

(f) The containment is purged with air and forced-air cooled.

(g) Sodium boils dry in the reactor cavity at 215 hours.

(h) Core debris (fuel and steel) penetrates the basement approximately 12 feet after dryout.

(i) Venting of the containment is stopped at 1000 hours (42 days).

While venting from the containment building is a part of the Inherent Retention concept the resultant radiological doses are to be within the guidelines of the NRC siting regulation, 10 CFR 100. The analysis of this approach by the plant applicant is still underway and it is expected that some, if not all, of the points raised here are receiving attention.

The computer code CACECO is relied upon to analyze the conditions within the plant itself after melt-through of the reactor vessel. The CACECO code is based on the CONTEMPT code prepared by the Phillips Petroleum Company in Idaho and has been modified at HEDL to more properly fit LMFBR problems. The code now considers conditions within each structural cell in the plant by taking account of fission products, spilled sodium (including chemical reactions) and energy transfer at the cell boundaries. Sodium boil-off, condensation, air injection, space cooling, concrete water release and venting can be treated by CACECO. It is generally necessary to follow the heat transfer processes for hundreds of hours with this code. The passage of sodium, reaction products, and moisture between cells, as permitted by the Inherent Retention concept, dictates that a computer code analysis is required. It has been strongly recommended that each large-scale sodium/concrete test be analyzed by CACECO so that every opportunity to spotlight code weaknesses is taken. The code has been implemented to reproduce

conditions found when relatively small amounts (hundreds of pounds) of sodium were released in a single concrete cell. Tests such as this one are used to establish empirical constants in the model.

Vent passages are present behind the steel liner in the reactor cavity to allow for disposal of moisture and CO_2 driven from the concrete when heated. The same passages may permit sodium to gain access to a very large concrete surface area with a large resultant energy release. The cavity sidewall liner needs additional consideration to assure that pressure or thermal effects do not cause a liner failure or permit sodium beneath the floor liner to pass up behind the sidewall liner. The 15 psig maximum pressure in the reactor cavity is capable of lifting liquid sodium up the floor vent line to approximately the level of the operating floor. Vent line voids would allow liquid sodium to spill directly onto the operating floor. Sodium may also solidify in the vent line thereby destroying vent effectiveness. Failure of the floor liner, which supports the heat generating fuel and steel, should be avoided while liquid sodium is present in the cavity.

The analysis of the third level margins in Reference 14 assumes that the core debris particulates when quenched by sodium in the reactor cavity. The particles are then assumed to self-level across the 40 foot diameter floor (forming a layer approximately one inch thick). The sodium pool would be quite effective in removing heat from such a shallow bed of debris. However, German workers have conducted tests with glass which indicate quenching of large, hot masses may not result in complete particulation. The self-leveling of debris beds has not been demonstrated to the extent assumed to occur. Incompleteness in either mechanism would lead to bed dry-out and local hot spots.

After sodium boils dry in the reactor cavity the fuel will self-heat to a high temperature and begin to melt its way downward into the concrete basemat

Reference 14 shows that the lowest melting poing eutectic of CaO (primary high temperature concrete constituent) and Fe_2O_3 (oxidized from rebar) occurs at 1200°C. The melting point of UO_2 alone is 2850°C and UO_2 and CaO from a eutectic which melts at 2060°C. Consideration should be given to the possibility that the partially molten fuel can penetrate the concrete basemat while covered by a solid UO_2 crust. It is expected that this would enhance the downward penetration above that described in the report which assumes rapid mixing of concrete melt and fuel. Figure 14 indicates the steady state thickness of liquid CaO and solid UO_2 which would separate solid concrete at 1200°C and liquid fuel at 2850°C (based on conduction alone).

Other aspects of the Inherent Retention concept which merit additional consideration include the degree of hydrogen non-uniformity in the containment atmosphere, the blockage of concrete/sodium reactions by the build-up in reaction products, thermal expansion accommodation in the steel liner, spalling of concrete and penetration of the cavity liner by streaming fuel. Following dryout in the reactor cavity it is assumed that 50% of the decay power is transferred to the concrete basemat. Penetration of the basemat is estimated to be 12 feet. No accounting is made of the other 50% of the decay power or its ultimate destination. The molten fuel pool will probably be covered by a layer of molten steel. This steel originally made up the pin cladding, duct walls, shield blocks, core support structure and vessel heads. If the fuel is diluted by molten concrete the pool density will drop below that of steel. If the steel layer moves to the bottom of the pool the penetration process in the concrete will be altered. This inversion process deserves attention. A complete listing of the issues raised with regard to third level margins is found in Reference 22.

5.3 Clinch River PSAR - Appendix F

Appendix F (title: Core Disruptive Accident Accommodation) of the Clinch River PSAR (Ref. 1) introduced special plant features to the baseline, or Reference design. The combination has been referred to as the Parallel Design. Within this appendix (and Appendix D) a core disruptive accident was treated as a design basis accident. The special plant features were introduced in Amendment 5 to the PSAR and continued to receive modification up through Amendment 17. The letter to the NRC (Ref. 23) which accompanied Amendment 5 pointed out that the applicant believed that further studies would indicate that the core disruptive accident should not be considered as a design basis accident. Subsequently, the applicant's letter to the NRC (Ref. 19) accompanying Amendment 18 stated that the Parallel Design efforts had been terminated and full confidence was being placed in the Reference Design (with several modification) as described in the main body of the PSAR. A conviction was expressed that the Reference Design suitably controlled the low probability initiators of severe accidents. The Parallel Design was not immediately withdrawn by the applicant in Amendment 18, because it was felt that the analysis contained in Appendix F would be useful in either design approach. However, in Amendment 24 (Ref. 24) the applicant withdrew Appendix D and large parts of F from consideration by the NRC staff. Amendments to the PSAR are being released on a continuing basis at the time of this writing. The NRC has not yet indicated it is willing to allow the deletion of the special plant features described in Appendix F. The comments and discussion which follow are directed at the Parallel Design as established by PSAR, Amendment 5-17.

UCLA, in its review capacity, has been most concerned with the heat and mass transfer problems following a core disruptive accident. Considerations

were both in-vessel and ex-vessel. When ex-vessel, attention centered around the core debris interaction with the sacrificial bed. (The bed is a special plant feature unique to the Parallel Design.) The full details of the Appendix F critique are in Ref. 25. Comments on the applicant's response to issues raised in the critique are in Ref. 26.

The design proposed for the sacrificial bed is shown in Figure 15. The bed is made up of MgO brick. A NaK active cooling system surrounds the bed perimeter and extends part way up the reactor cavity sidewall. Core debris is to drop into the shallow receptacle in the top of the bed. Poison rods and a separator dome assist in preventing recriticality. The decay energy contained in the debris is to be absorbed by melting of the bed and by conduction into the active cooling system. The molten pool should not reach the bed boundaries.

The height of the sidewall cooling system in the reactor cavity should be increased. Sodium vapor pressure within the failed reactor vessel may depress the sodium surface within the guard vessel skirt; raising it outside the guard gessel. No consideration is given in Appendix F to non-uniformities in the surface temperature of the sodium. A hot plume is expected to develop near the cavity centerline. The ullage vapor pressure will be set by the local surface temperature created by this plume. The quenching action of the sodium on the molten fuel and steel needs additional study. German workers have shown that large molten masses do not always completely particulate when quenched. The debris will not readily self-level nor remain wetted if not finely divided into particles.

Molten pool growth in the sacrificial bed has been predicted by using computer codes GROWS (Ref. 5) and AYER (Ref. 8). The applicant used GROWS to bracket the portion of the decay energy transferred to the bed rather than

into the overlying sodium pool. The fraction propagating downward was then an input to the finite-element code AYER. This latter code followed the growth of the molten pool until freezing commenced (with allowance for conduction into the active cooling system). The maximum pool size was 3200 cubic feet (depth: 8 ft) when 70% of the decay energy was directed into the bed. Pool growth ceased after 18 days. The analysis assumes rapid mixing of the MgO melt with the molten fuel. This solubility rate should be examined experimentally as existing data is meager. The division of downward moving decay energy into outward and downward components in the bed deserves added attention. High outward (to pool sidewall boundaries) heat flux may bring the molten pool boundary to the extreme edge of the sacrificial bed. The Appendix F discussion does not address the possibility of a fuel or steel crust on the molten debris pool. The resistance of the MgO powder layer in the bed receptacle should be quantified. The impingement of the hot, dense debris stream may sweep it away, destroying its ability to absorb thermal shock. No mention is made of the possibility that molten steel could move to the bottom of the fuel/MgO pool when the pool density has been reduced.

Several issues have been raised at UCLA pertaining to core debris behavior within the reactor vessel. The manner in which a molten fuel pool can cause failure of the lower reactor vessel head is unclear. Reineke (Ref. 27) has indicated that his experiment show maximum heat transfer at the upper surface of the pool; not at the bottom. Such a development may lead to asymmetric loading of the sacrificial bed. The question of complete debris particulation by sodium (in the lower plenum) has already been raised. Experiments at UCLA (Ref. 17) have been concerned with dry-out heat flux in a self-heated debris bed. The results are at variance with the predictions made in Appendix F (see Section 4.3). Debris bed dry-out limits the amount of core debris which

can be held in a thermally stable state on the various horizontal surfaces within the reactor vessel.

A portion of the analysis described in Appendix F is supported by Reference 7. This report adds details to the molten pool growth prediction process and the time required to melt through the reactor vessel. Additional comments on that presentation are outlined in Ref. 28.

6.0 AEROSPACE CORPORATION TA PROGRAM SUPPORT

A large number of complex material interactions are involved in a core meltdown accident in a liquid metal fast breeder reactor. Many of the interactions take place at high temperature (up to 3500°C) and have not been previously studied. The materials which may be involved include, but are not limited to, very large amounts of fuel (UO_2 and PuO_2), steel, sodium, concrete and various refractory materials such as MgO firebrick. The sequence and fashion in which these materials come together is dependent upon the path taken by the molten core following a core disruptive accident. The consequences of the various interactions are reflected in the rate of release of fission products initially contained in the core debris. Scenarios have been proposed to describe the sequence of interactions by several authors (Ref. 7 and 29) but no one is prepared to say that any description is definitive.

The Aerospace Corporation (a non-profit organization established by the Air Force) has a strong research background in studying the high temperature performance of materials. This work has been carried out within the Materials Sciences Laboratory with its high temperature material testing facility. In addition to assisting the Air Force, the Aerospace Corporation has made its materials expertise available to other governmental agencies. Laboratory personnel and facilities are commonly used to provide quick answers in problem areas which demand immediate answers.

The Division of Project Management within the Nuclear Regulatory Commission has gone to the Aerospace Corporation for assistance in its licensing program for the Clinch River Plant. The objective is to conduct confirmatory materials research at Aerospace to substantiate information provided by the plant license applicant. The program is titled "Ex-Vessel Core Catcher Mater-

ials Interaction Program" and was initiated in December 1975. Primary emphasis is to be on experimental research in the Materials Sciences Laboratory using actual reactor materials on a small scale. The NRC has also asked UCLA to become involved in the Aerospace program and assist in experimental sizing. UCLA will provide a thermo-hydraulic input and help in scaling the findings to the reactor situation. The results will also be used as inputs to the computer models which are being used to assess the safety adequacy of the Clinch River Plant. The first high temperature tests using depleted uranium dioxide were carried out in the second quarter of CY 1976.

The full application of the knowledge gained is intended to permit the NRC to make an independent evaluation of core disuprive accidents and their potential consequences.

Principal safety areas of concern with respect to licensing the Clinch River Breeder Reactor Plant are:

a) Core debris interactions with sacrificial bed materials such as MgO.

b) Sodium-concrete reactions.

c) Sodium interactions with steel-lined concrete walls.

d) Core debris interaction with steel-lined concrete walls.

The first item has application to the CRBRP Parallel Design within which a large (40 ft dia, 12 ft thick) sacrificial bed sets in the bottom of the reactor cavity. The other three items are pertinent to the Parallel Design but more so to the alternate design proposal referred to as the Inherent Retention Concept. This latter design deletes the sacrificial bed and incorporates other safety features including hot and cold steel liner shields in the concrete reactor cavity. The Aerospace test program is directed toward each of these four areas of concern.

The first series of interaction tests will take place in an arc-furnace. The electric arc will be used to melt depleted UO_2 within a graphite crucible. Steel may also be present in this melt. The molten material will be poured out of the crucible and onto materials such as concrete, refractory brick or steel plate. The tests will be transient in nature at first. After cooling the specimens will be sectioned and examined physically using various microscopic techniques and examined for chamical constituents using the ion-microprobe, mass analysis. Optical and thermocouple temperature measurements will be made. The matrix shown in Table VII outlines the first ten tests to be conducted using the arc furnace.

TABLE VII

Materials Interaction Test Matrix

Test No.	Molten Pour Material	Base Material	Test Duration
1	UO_2	MgO	Transient
2	2/3 UO_2 + 1/3 S.S.	"	"
3	S.S.	"	"
4	2/3 UO_2 + 1/3 S.S.	Carbon Steel Plate	"
5	"	S.S. Plate	"
6	UO_2	Concrete	"
7	2/3 UO_2 + 1/3 S.S.	"	"
8	S.S.	"	"
9	2/3 UO_2 + 1/3 S.S.	MgO	Steady State
10	"	Concrete	"

The mixture range between UO_2 and steel is intended to encompass that which would be present if the core, lower axial blanket, and first row of the radial blanket melted. The variation in steel present is due to the uncer-

tainty in the amount of shield block, support plate, reactor vessel, and guard vessel which would add to the molten debris prior to dropping out of the failed guard vessel.

A transient thermal conduction analysis was made to determine the minimum duration for the steady-state tests (#9, #10). As a guideline that time was chosen for which the specimen midplane temperature rose to one-half the upper surface melting temperature. This time is given by (see Ref. 30, page 149) $0.23\ell^2/\alpha$ where ℓ is the specimen thickness and α is its thermal diffusivity. This minimum time calculation yields approximately 15 minutes for MgO (α = 0.065 ft^2/hr) and 35 minutes for concrete (α = 0.025 ft^2/hr) if the specimen is three inches thick. Continuous heating for the steady state tests will be provided by holding the arc over the molten UO_2/steel pool.

Radiative losses from the surface of the hot molten pool account for the major portion of the energy input from the arc. For example, at a surface temperature of 3500°C and a surface emissivity of 0.8 the radiation loss from a pool surface of 40 cm^2 is estimated to be 35 kw based on an idealized geometry. Radiation shields have been considered but no suitable design has been proposed which allows the operator room to see and maneuver the arc electrode at the pool surface.

UCLA support of the Aerospace materials interaction program is an on-going effort. As results from the test program become available UCLA will assist in interpretation of the findings and extrapolation to the full-scale reactor situation.

REFERENCES

1. _____"Clinch River Breeder Reactor Plant (CRBRP) Preliminary Safety Analysis Report (PSAR)", Project Management Corp., 1975

2. Russell, H. W., "Principles of Heat Flow in Porous Insulators", Amer. Ceramic Society J., Vol. 18, 1935

3. Kingery, W. O. et al, "Thermal Conductivity:X, Data for Several Pure Oxide Materials Corrected to Zero Porosity", Amer. Ceramic Society J., Vol. 37, 1954

4. Lambe and Whitman, Soil Mechanics, John Wiley and Sons, New York, 1969, p. 281-289

5. Kumar, R. et al, "Ex-Vessel Considerations in Post accident Heat Removal", Argonne National Laboratory, ANL/RAS 74-29, Oct. 1974

6. Fardahieh, "Simulation of Pool Growth in Sacrificial-Material Beds", Argonne National Laboratory, ANL-RDP-44, Oct. 1975

7. Birmingham, D. et al, Ex-Vessel Core Catcher Concept Evaluation Report", Westinghouse Electric Corp., WARD-D-0103, Oct. 1975

8. Lawton, R. G., "The AYER Heat Conduction Computer Program", Los Alamos Scientific Laboratory, LA-5613-MS, May 1974

9. Dhir, V. K. et al, "Role of Wall Heat Transfer and Other System Variables on Fuel Compaction and Recriticality" Paper presented at International Meeting on Fast Reactor Safety and Related Physics, Chicago, Oct. 1976

10. Taylor, G. I., "The Instability of Liquid Surfaces when Accelerated in a Direction Perpendicular to Their Planes, Part I", Proc. Roy. Soc. London, A-201, 1950

11. Zuber, N., "Hydrodynamic Aspects of Boiling Heat Transfer", AEC Report AECU-4439, Physics and Mathematics, 1959

12. Berenson, P. J., "Film Boiling Heat Transfer from a Horizontal Surface" J. Heat Transfer, Trans ASME, Series C, Vol. 83, 1961

13. Baker, L., et al", Post Accident Heat Removal in Fast Reactors:, Argonne National Lab., ANL/RAS 75-44, November, 1975

14. _____"Third Level Thermal Margina in the CRBRP", Project Management Corp., April 1975

15. Miyazaki, H. and E. Silberman, "Flow and Heat Transfer on a Plate Normal to Two-Dimensional Laminar Jet...", J. Heat Mass Transfer, Vol. 15, 1972

16. Johnson, T. R., et al, "Post Accident Heat Removal - Large Scale Fuel-Sodium Interaction Experiments", Argonne Nat'l. Lab., ANL/RAS 74-1, Feb. 1974

17. Catton, I, "Post Accident Heat Removal for LMFBR's", Univ. of Calif., Los Angeles, UCLA-ENG-7593, 1975

18. Dhir, V. J. and Catton, I., "Dryout Heat Fluxes in Beds of Volumetrically Heated Particles," University of California, Los Angeles, UCLA-ENG-7678, to be published

19. Letter, P. S. Van Nort (Gen. Manager, Project Management Corp.) to R. S. Boyd (Director, NRC) April 30, 1976

20. Letter, W. Kastenberg, to T. Speis, March 5, 1976

21. Letter, W. Kastenberg to T. Speis, May 10, 1976

22. Letter, J. Castle to A. Marchese, May 27, 1976

23. Letter, R. E. Jortberg (Assistant Gen. Manager, Project Management Corp.) to R. S. Boyd, Oct. 6, 1975

24. Letter, A. R. Buhl (Assistant Director for Public Safety, ERDA) to R. S. Boyd (Director, NRC), July 22, 1976

25. Letter, J. Castle to A. Marchese, November 14, 1975

26. Letter, J. Castle to A. Marchese, June 15, 1976

27. Reineke, H. H. and M. Jahn, "Free Convection Heat Transfer with Internal Heat Sources, Calculations and Measurements", NC 218, Fifth International Heat Transfer Conf., Japan, 1974

28. Letter, J. Castle to A. Marchese, February 10, 1976

29. Gluekler, E. L., "Status of Core-Meltdown Consequence Evaluation for Early-Sized LMFBR", General Electric Co., 1975

30. Krieth, F. "Principles of Heat Transfer", International Textbook Co., PA, Second Ed. 1965

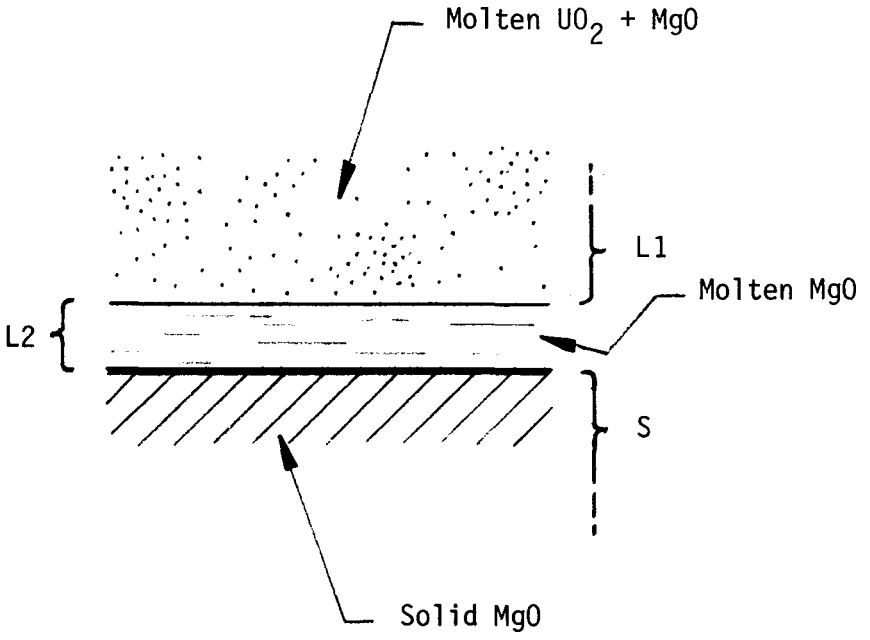

Figure 1. Sacrificial Bed Layer Model

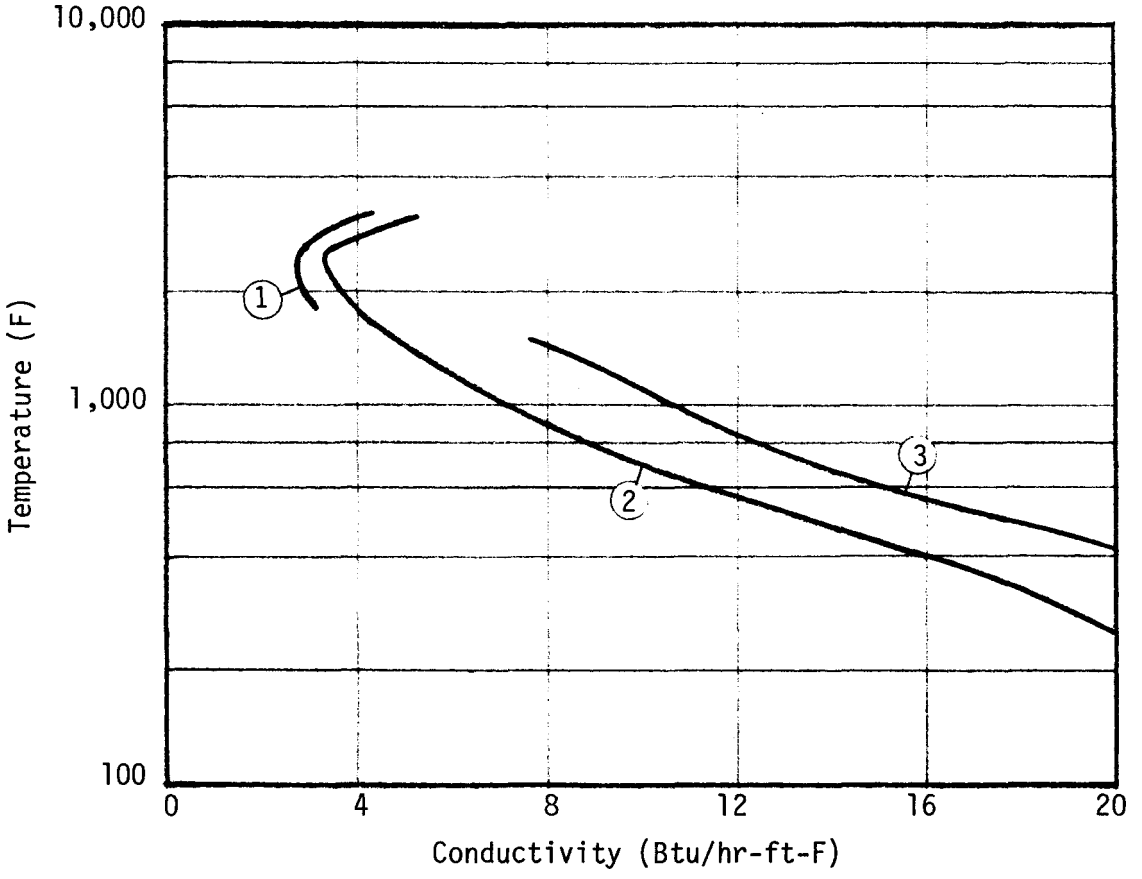

Curve 1. MgO saturated with Na vapor
2. MgO alone
3. MgO saturated with Na liquid

FIGURE 2. SACRIFICIAL BED BRICK CONDUCTIVITY

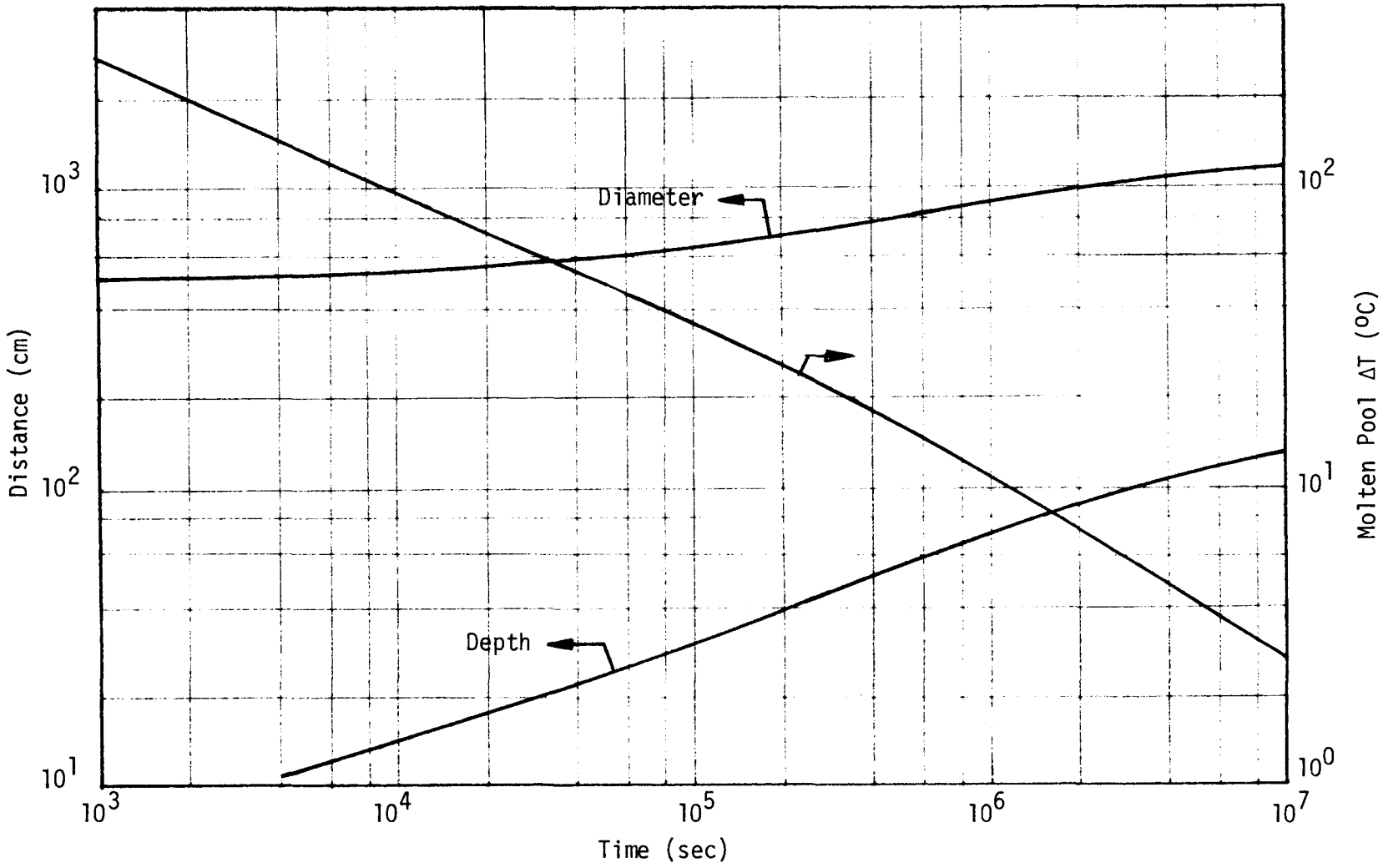

FIGURE 3. "GROWS" PREDICTION OF POOL GROWTH IN A MgO BED

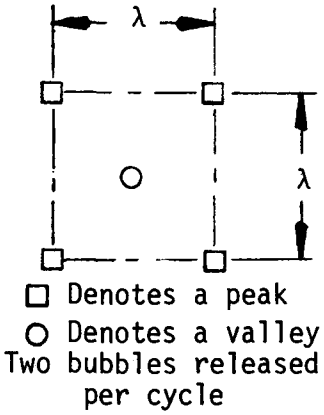

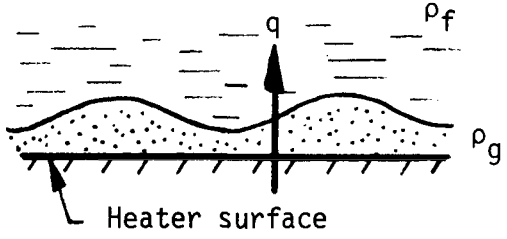

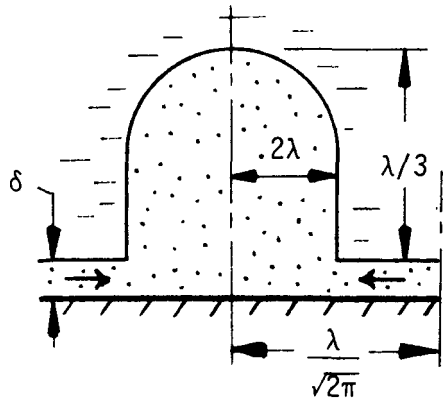

A. Zuber-Berenson Model

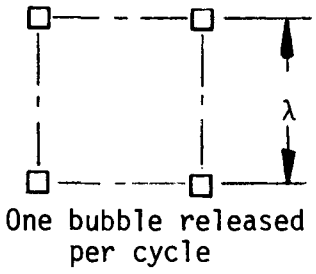

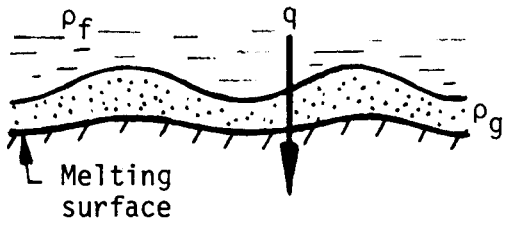

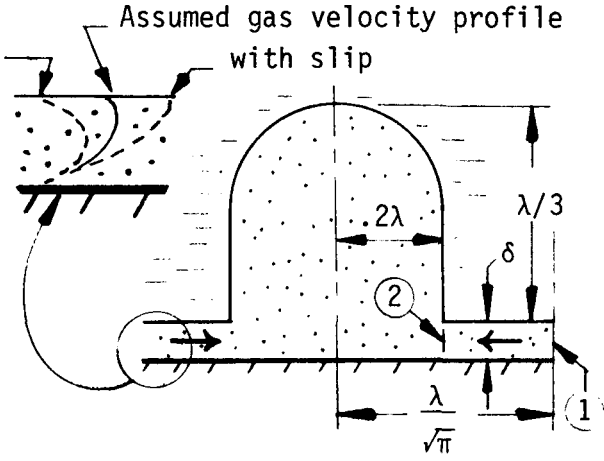

B. Pseudo-Film Boiling Model

FIGURE 4. FILM BOILING MODELS

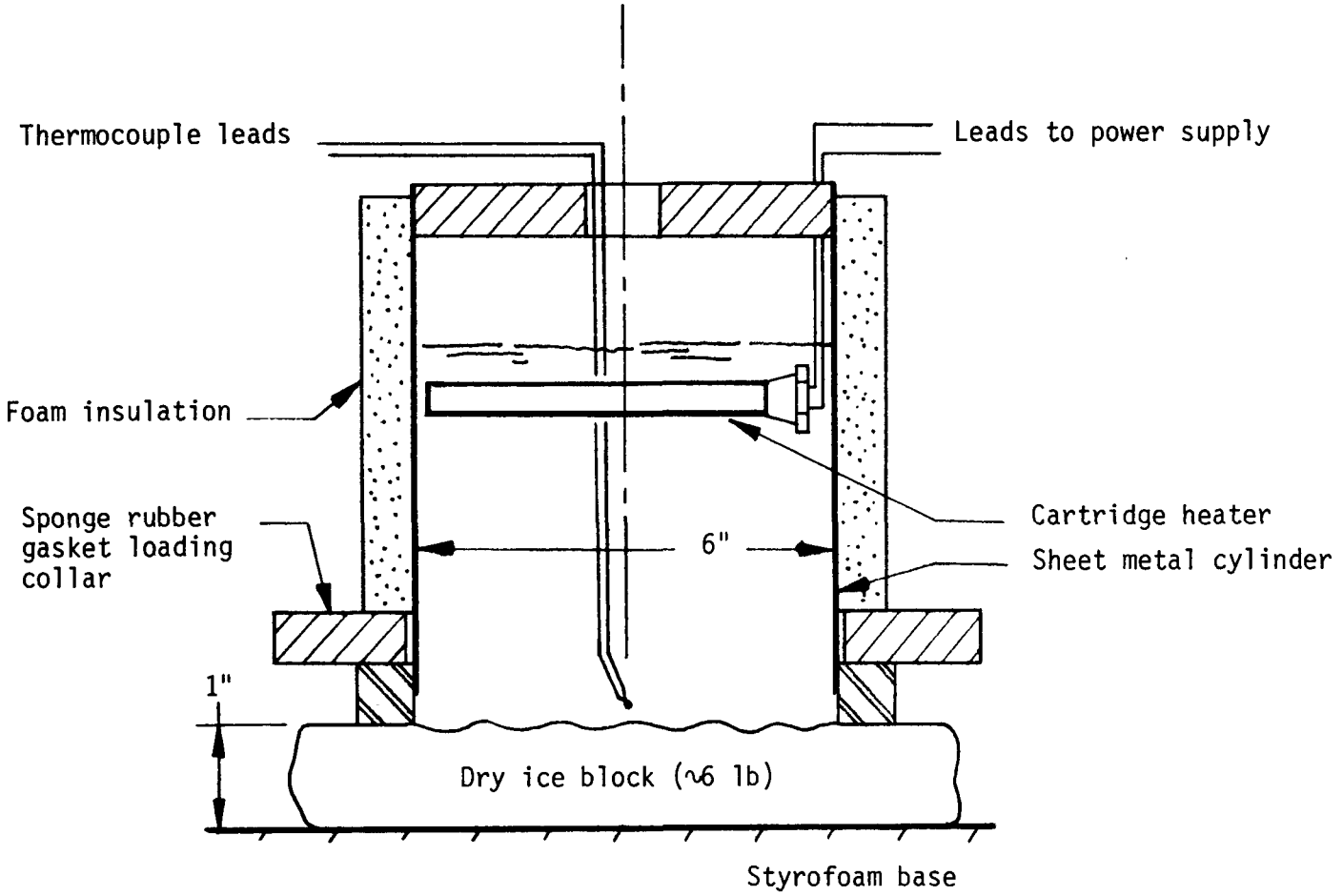

FIGURE 5. TEST APPARATUS

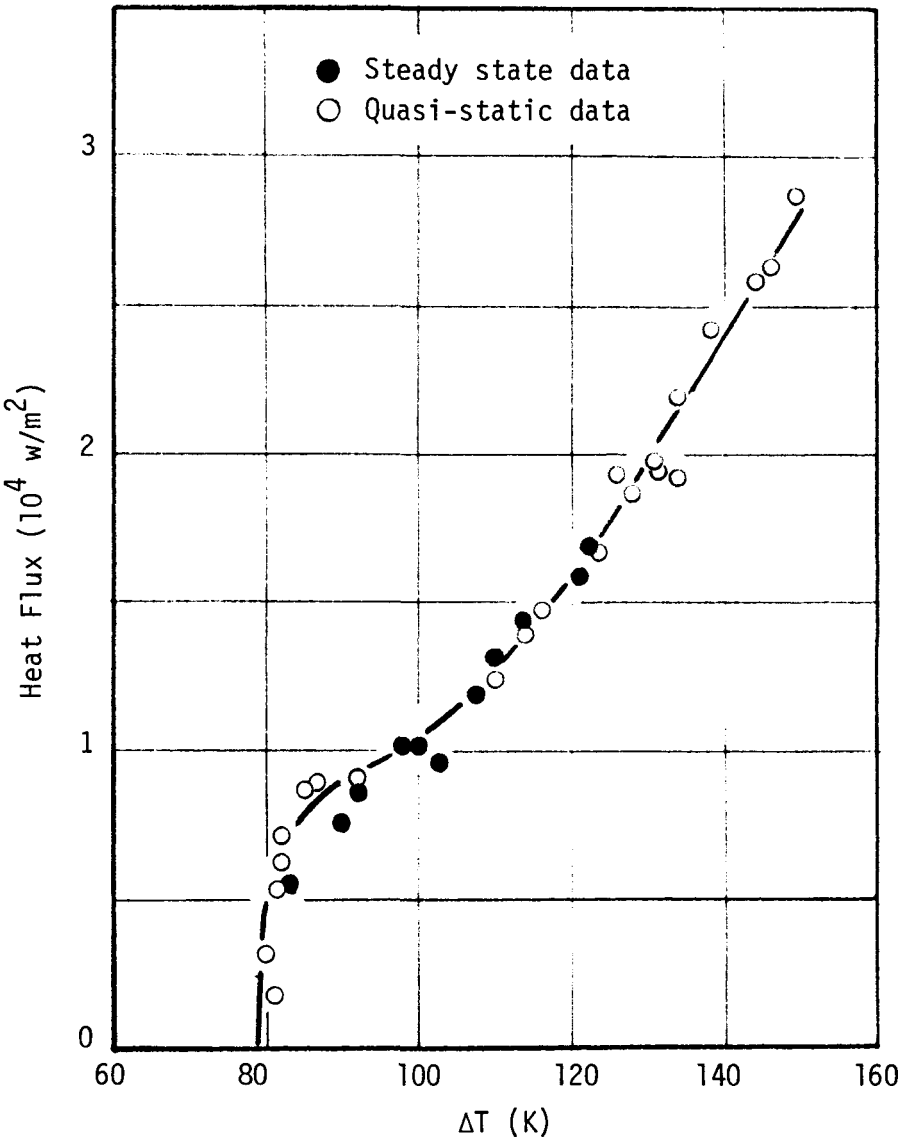

FIGURE 6. VARIATION OF HEAT FLUX WITH TEMPERATURE FOR DRY ICE-WATER SYSTEM

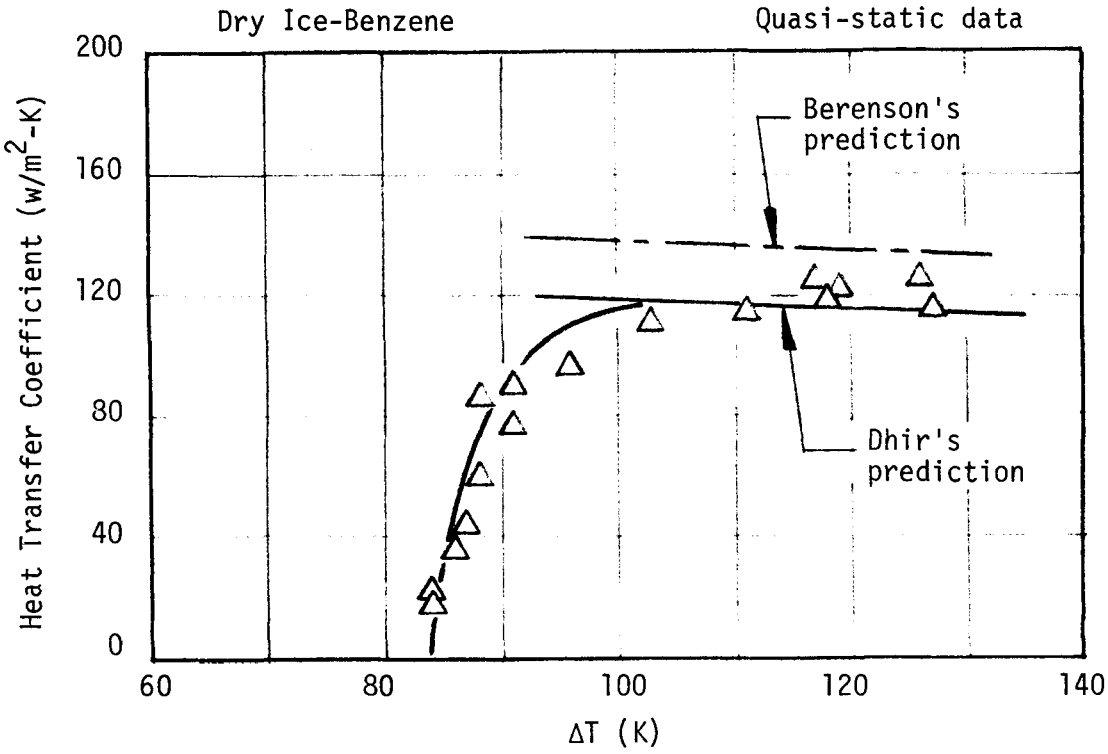

FIGURE 7. VARIATION IN HEAT TRANSFER COEFFICIENT WITH TEMPERATURE

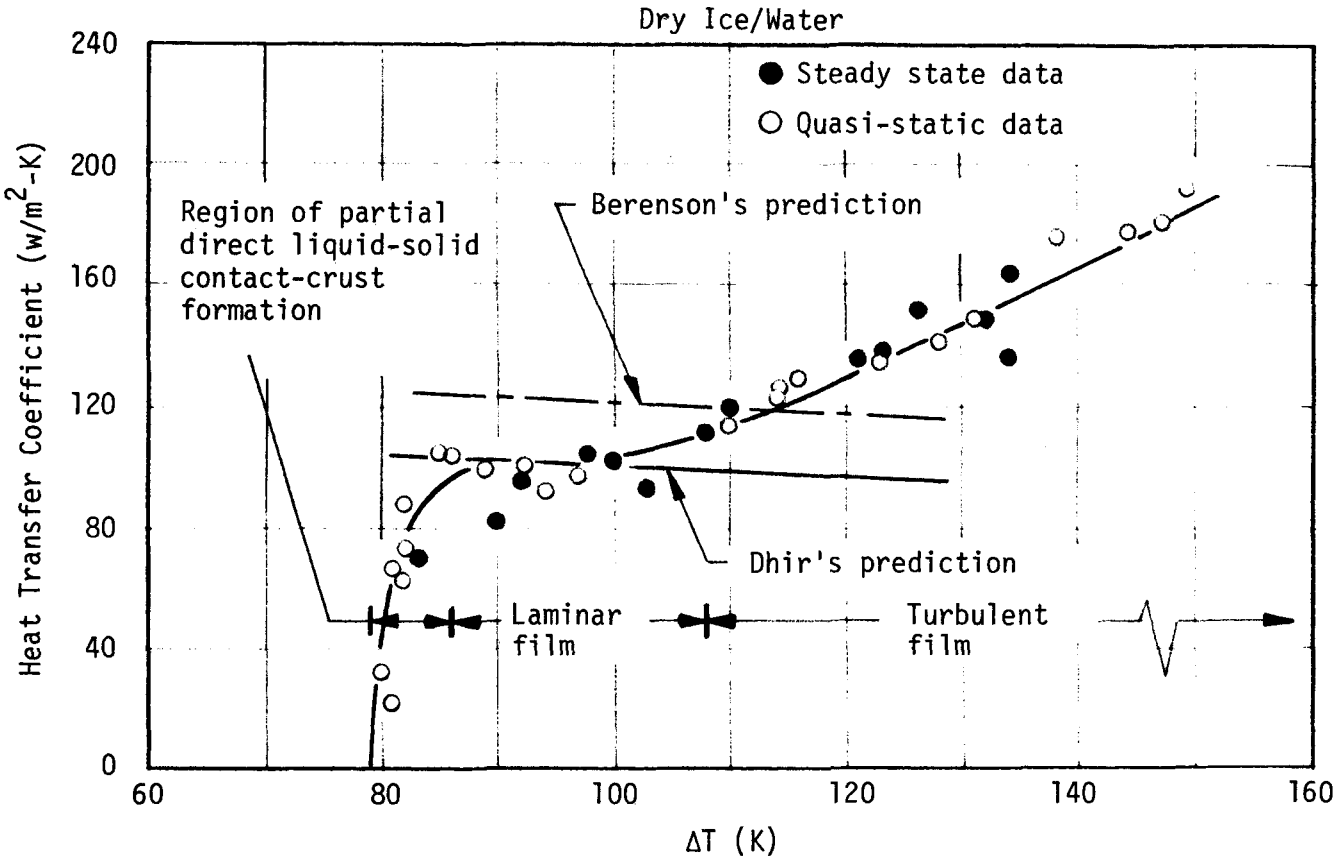

FIGURE 8. VARIATION OF HEAT TRANSFER COEFFICIENT WITH TEMPERATURE

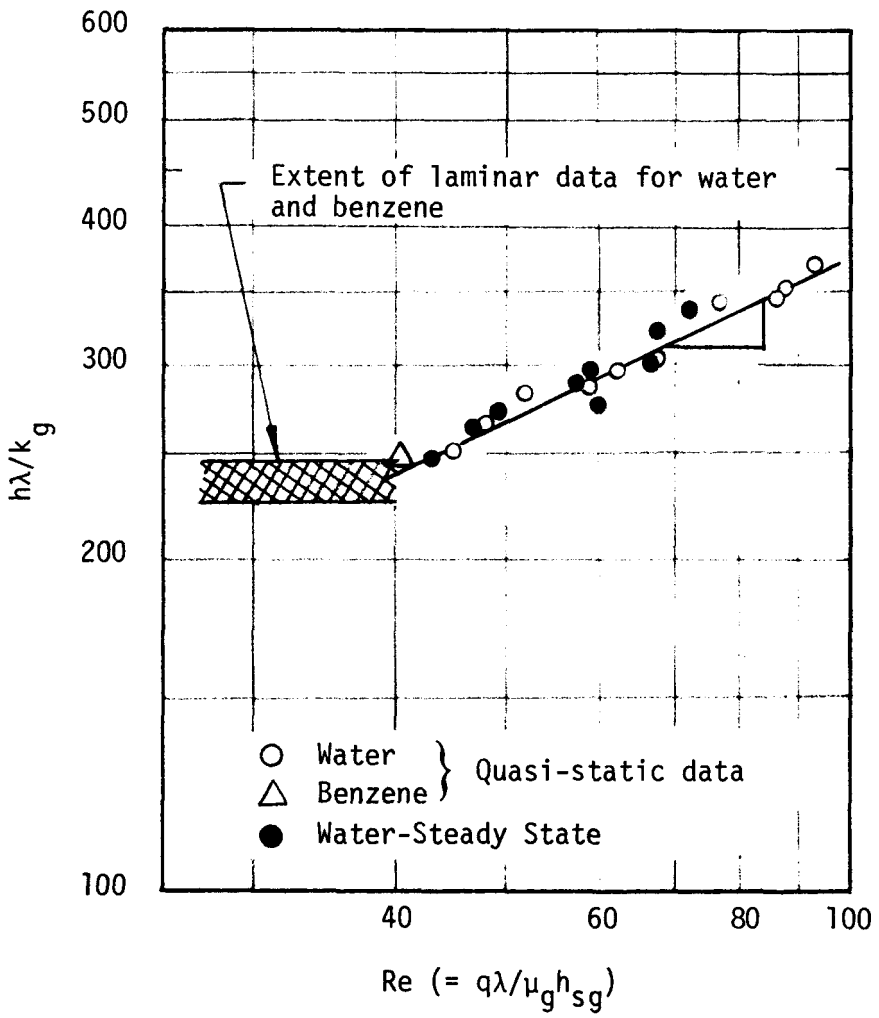

FIGURE 9. DEPENDENCE OF PSEUDO-FILM BOILING HEAT TRANSFER COEFFICIENT ON REYNOLDS NUMBER

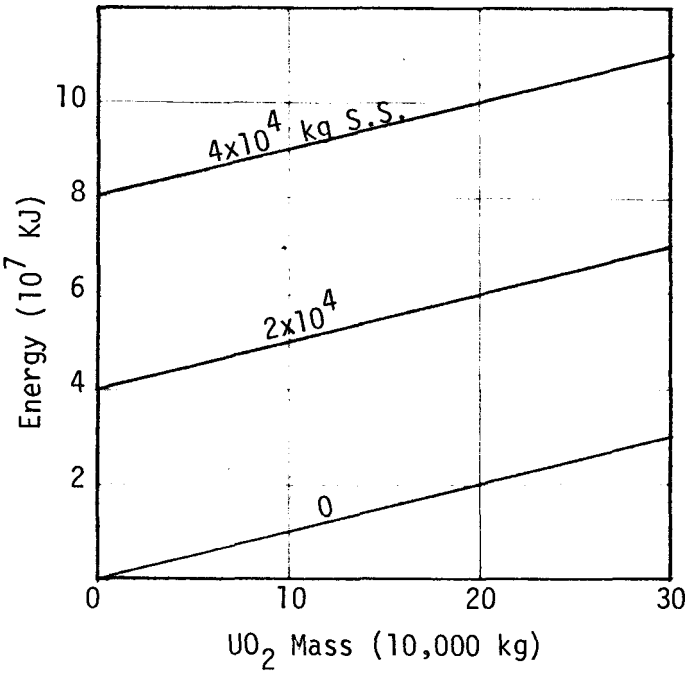

FIGURE 11 ENERGY REQUIRED TO REMELT FUEL AND STEEL IN DEBRIS

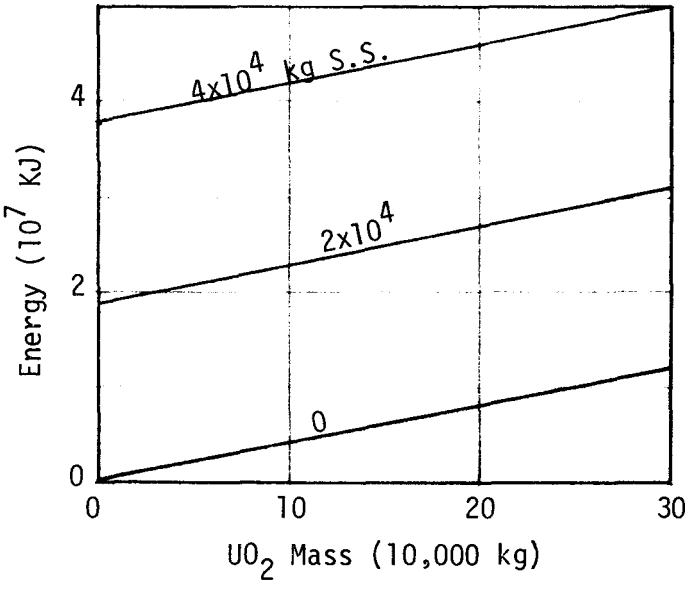

FIGURE 10 ENERGY REQUIRED TO REMELT STEEL IN DEBRIS

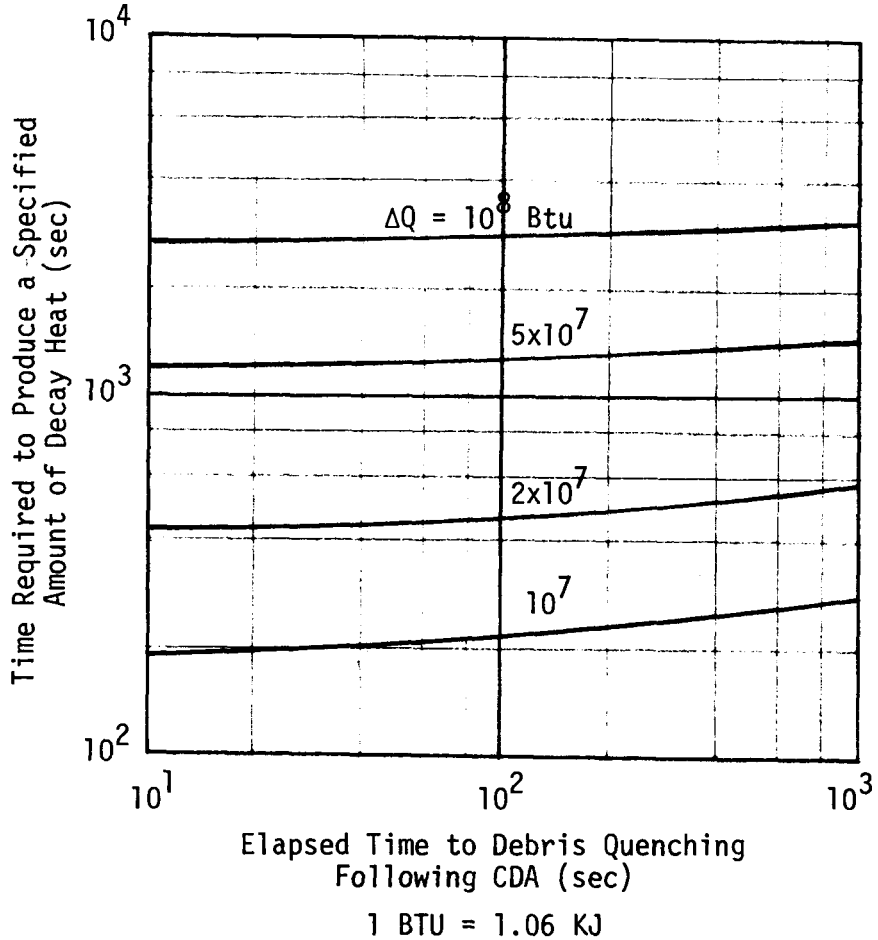

FIGURE 12. DEBRIS BED REMELT TIME

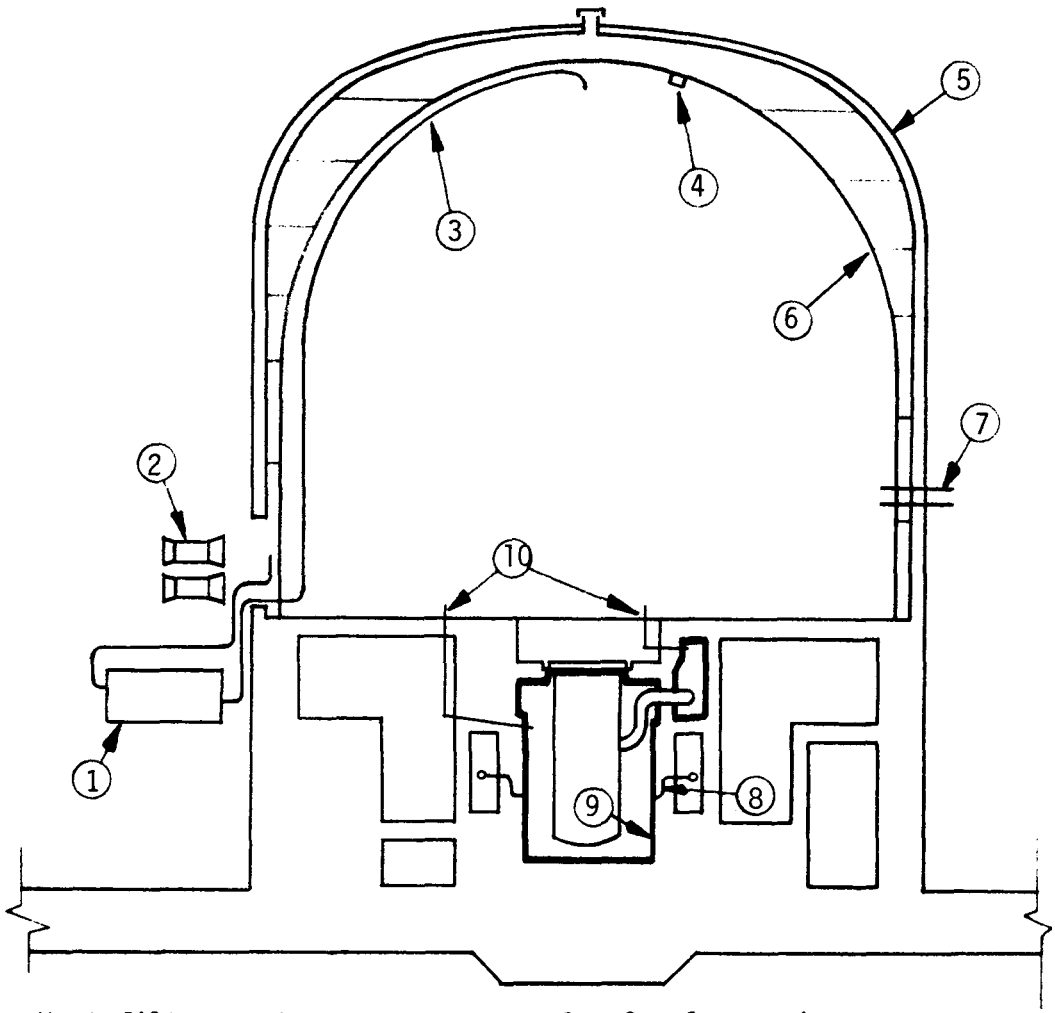

1. Vent filter system
2. Annulus cooling fans
3. Containment vent line
4. Instrumentation
5. Concrete confinement
6. Steel containment
7. Air purge inlet
8. Liner vent
9. Inner barrier
10. Sodium vent

FIGURE 13. THIRD LEVEL DESIGN FEATURES

CONDUCTION MODEL

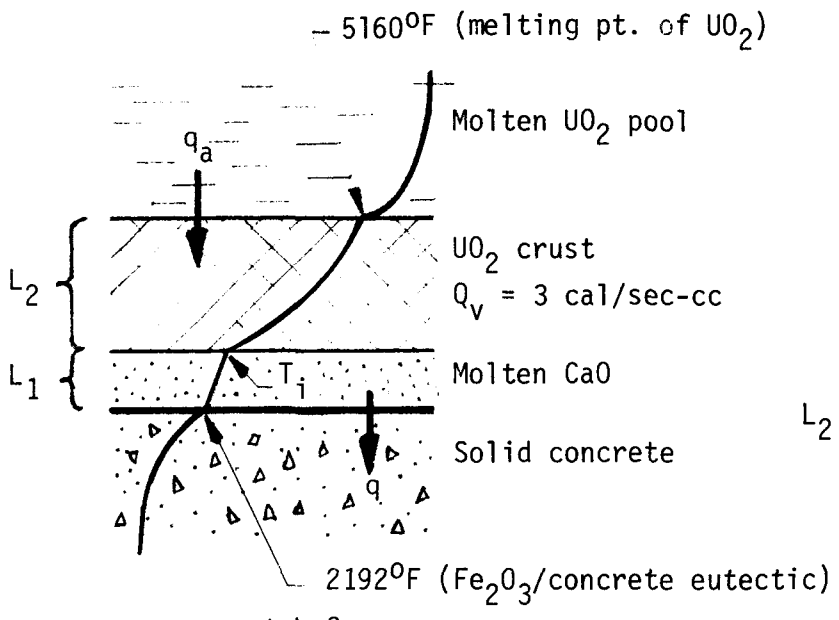

$q = q_a + L_2 Q_v$

$k_1 = 0.35$ Btu/hr-ft-°F

$k_2 = 1.7$

$T_{i_{max}} = 3740°F$ (UO_2/CaO eutectic)

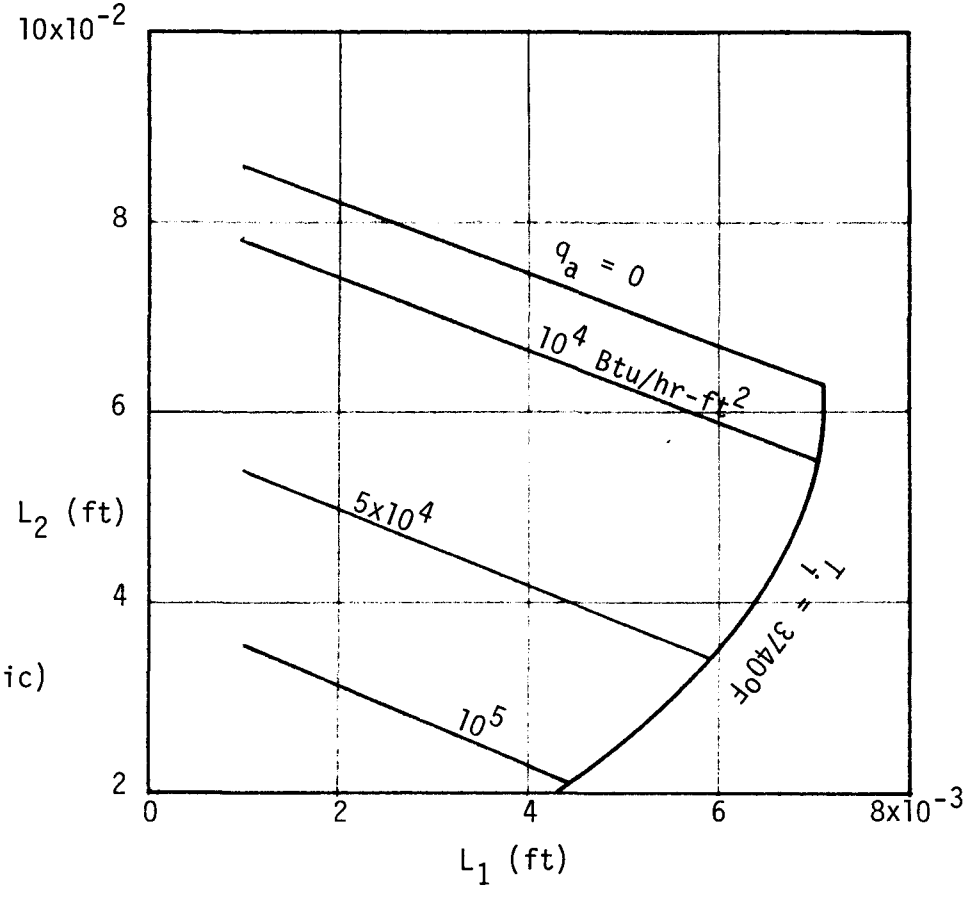

FIGURE 14. CRUST FORMATION ABOVE CONCRETE

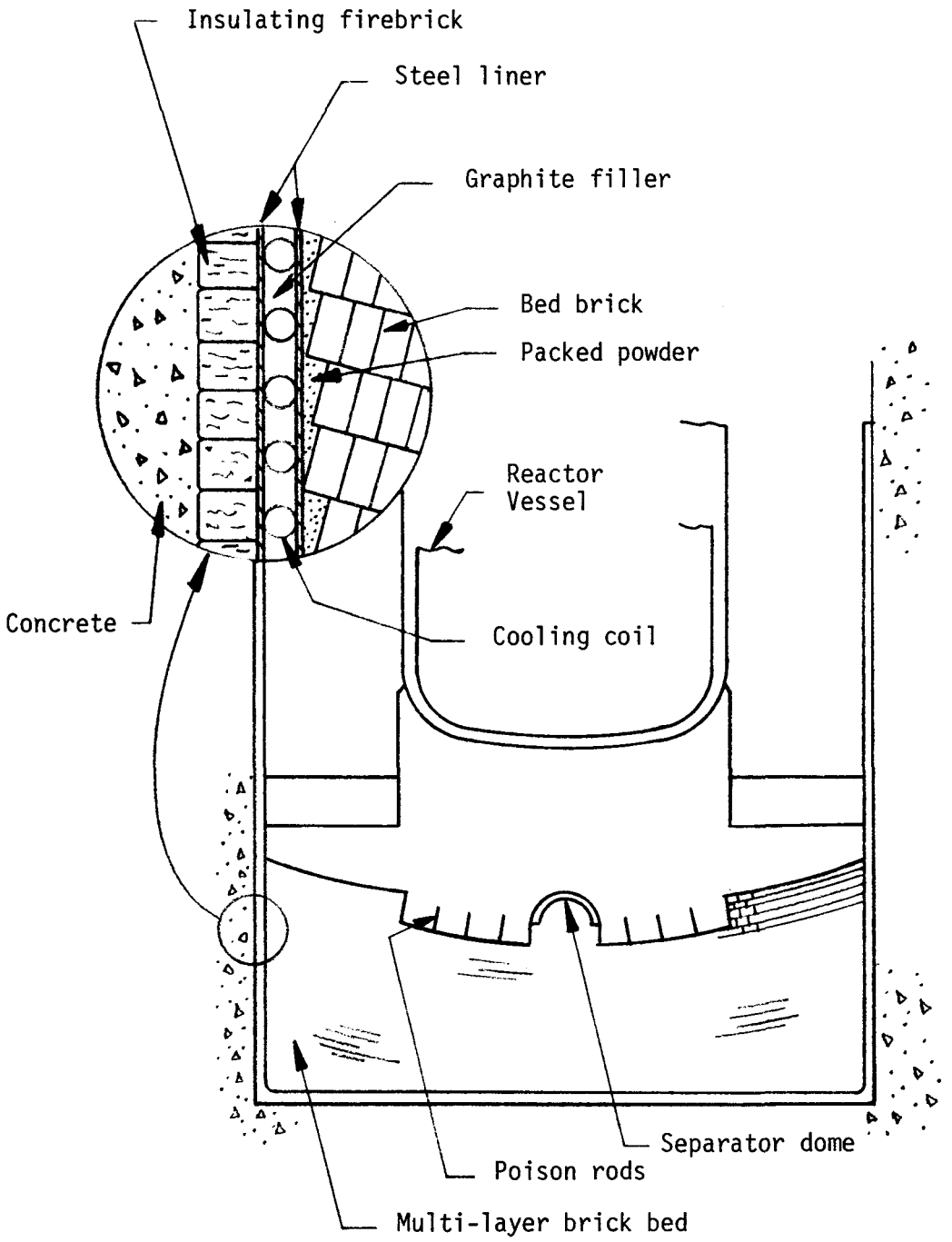

FIGURE 15. SACRIFICIAL BED CONCEPT